Cell Reports
Medicine

Article

Prime editing functionally corrects cystic fibrosis-causing *CFTR* mutations in human organoids and airway epithelial cells

Graphical abstract

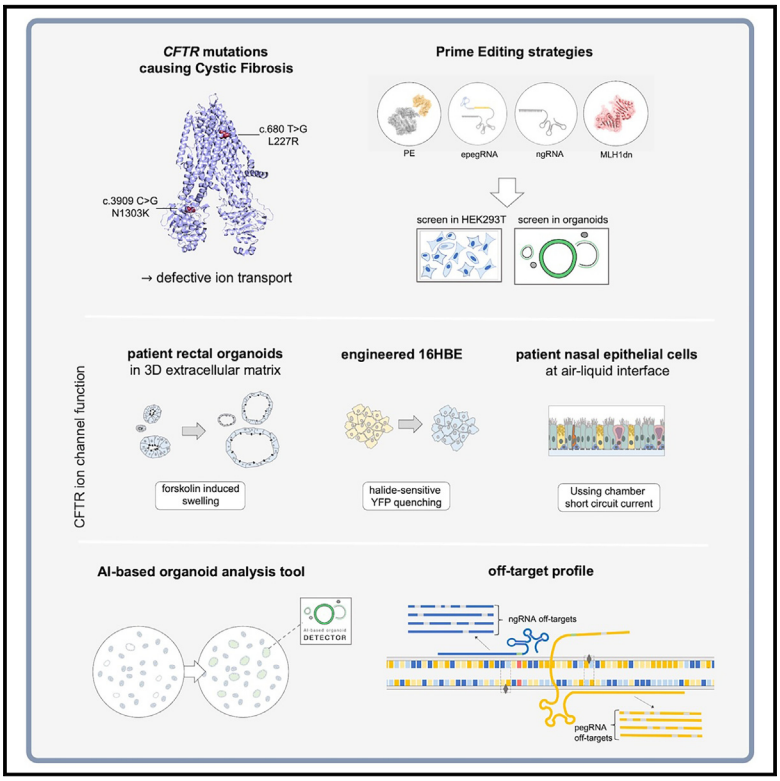

Highlights

- Prime editing can be used to precisely correct cystic fibrosis-causing mutations
- Efficient functional correction in patient-derived organoids and airway epithelium
- Machine learning tool DETECTOR functionally screens genetic strategies in primary organoids
- Genome-wide evaluation of prime editing for L227R and N1303K confirms high fidelity

Authors

Mattijs Bulcaen, Phéline Kortleven, Ronald B. Liu, ..., Isabelle Sermet-Gaudelus, Anna Cereseto, Marianne S. Carlon

Correspondence

mattijs.bulcaen@kuleuven.be (M.B.), marianne.carlon@kuleuven.be (M.S.C.)

In brief

Bulcaen et al. develop prime editing strategies to correct L227R- and N1303K-CFTR, two drug-ineligible mutations causing cystic fibrosis. Delivery of all components to patient-derived rectal organoids and human nasal epithelial basal cells leads to genetic and functional correction without any detectable off-target editing events.

Bulcaen et al., 2024, Cell Reports Medicine *5*, 101544
May 21, 2024 © 2024 The Authors. Published by Elsevier Inc.
https://doi.org/10.1016/j.xcrm.2024.101544

CellPress

Cell Reports Medicine

CellPress
OPEN ACCESS

Article

Prime editing functionally corrects cystic fibrosis-causing *CFTR* mutations in human organoids and airway epithelial cells

Mattijs Bulcaen,[1,2,*] Phéline Kortleven,[2] Ronald B. Liu,[3,4] Giulia Maule,[5] Elise Dreano,[6,7] Mairead Kelly,[6,7] Marjolein M. Ensinck,[2] Sam Thierie,[2] Maxime Smits,[1,8] Matteo Ciciani,[5] Aurelie Hatton,[6,7] Benoit Chevalier,[6,7] Anabela S. Ramalho,[9] Xavier Casadevall i Solvas,[3] Zeger Debyser,[1,8] François Vermeulen,[9,10] Rik Gijsbers,[1,8] Isabelle Sermet-Gaudelus,[6,7,11,12] Anna Cereseto,[5] and Marianne S. Carlon[2,8,13,*]

[1]Department of Pharmaceutical and Pharmacological Sciences, KU Leuven, 3000 Leuven, Belgium
[2]Department of Chronic Diseases and Metabolism, KU Leuven, 3000 Leuven, Belgium
[3]Department of Biosystems, KU Leuven, 3000 Leuven, Belgium
[4]School of Engineering, University of Edinburgh, EH9 3JL Edinburgh, UK
[5]Department of CIBIO, University of Trento, 38123 Povo-Trento, Italy
[6]INSERM, CNRS, Institut Necker Enfants Malades, 75015 Paris, France
[7]Université Paris-Cité, 75015 Paris, France
[8]Leuven Viral Vector Core, KU Leuven, 3000 Leuven, Belgium
[9]Department of Development and Regeneration, KU Leuven, 3000 Leuven, Belgium
[10]Department of Pediatrics, UZ Leuven, 3000 Leuven, Belgium
[11]Cystic Fibrosis National Pediatric Reference Center, Pneumo-Allergologie Pédiatrique, Hôpital Necker Enfants Malades, Assistance Publique Hôpitaux de Paris (AP-HP), 75015 Paris, France
[12]European Reference Network, ERN-Lung CF, 60596 Frankfurt am Mein, Germany
[13]Lead contact
*Correspondence: mattijs.bulcaen@kuleuven.be (M.B.), marianne.carlon@kuleuven.be (M.S.C.)
https://doi.org/10.1016/j.xcrm.2024.101544

SUMMARY

Prime editing is a recent, CRISPR-derived genome editing technology capable of introducing precise nucleotide substitutions, insertions, and deletions. Here, we present prime editing approaches to correct L227R- and N1303K-CFTR, two mutations that cause cystic fibrosis and are not eligible for current market-approved modulator therapies. We show that, upon DNA correction of the *CFTR* gene, the complex glycosylation, localization, and, most importantly, function of the CFTR protein are restored in HEK293T and 16HBE cell lines. These findings were subsequently validated in patient-derived rectal organoids and human nasal epithelial cells. Through analysis of predicted and experimentally identified candidate off-target sites in primary stem cells, we confirm previous reports on the high prime editor (PE) specificity and its potential for a curative CF gene editing therapy. To facilitate future screening of genetic strategies in a translational CF model, a machine learning algorithm was developed for dynamic quantification of CFTR function in organoids (DETECTOR: "detection of targeted editing of *CFTR* in organoids").

INTRODUCTION

Cystic fibrosis (CF) is one of the most common inherited lethal diseases and has an estimated worldwide prevalence of >160,000 patients.[1] Perhaps the archetype of an autosomal recessive disorder, CF is caused by biallelic loss-of-function mutations in the *CFTR* gene. More than 2,000 mutations have been identified, of which >700 have been confirmed to be disease causing.[2] *CFTR* codes for CF transmembrane conductance regulator, a chloride and bicarbonate channel present in the apical plasma membrane (PM) of cells lining epithelial surfaces.[3] In people with CF (pwCF), loss of CFTR protein production or function manifests as a disrupted water-salt balance in several organs. In the lungs, failure to produce mobile mucus leads to airway obstruction, microbial colonization, chronic inflammation, and progressive lung damage.[3] Tremendous progress has been made since the discovery of the *CFTR* gene in 1989,[4–6] which has led to the approval of four CFTR modulator therapies over the past 12 years (reviewed in Ensinck and Carlon[7]).

Highly effective modulator therapies (HEMTs) that aid mutated CFTR protein in folding and gating received market approval for pwCF with at least one F508del allele or another responsive *CFTR* mutation. F508del constitutes 60%–70% of all alleles in the US and European registries and hence renders all other mutations rare in comparison.[2] However, recent evidence suggest that non-F508del mutations are much more common outside non-Hispanic White populations, where CF

This is an open access article under the CC BY-NC-ND license (http://creativecommons.org/licenses/by-nc-nd/4.0/).

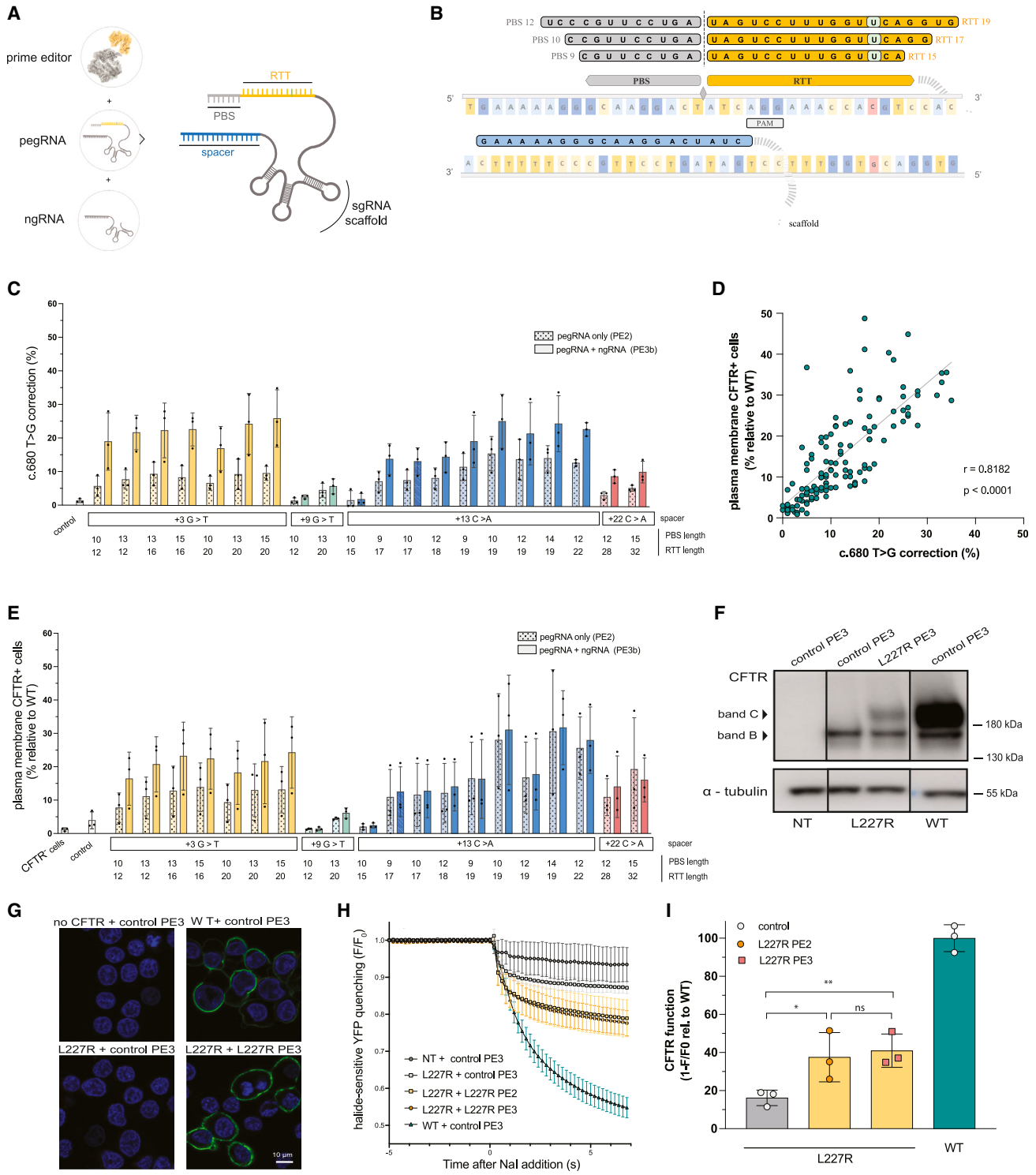

Figure 1. Prime editing of c.680T>G (L227R) rescues CFTR glycosylation, PM localization, and anion channel function

(A) PE3 strategies require delivery of the prime editor (PE) enzyme, prime editing guide (pegRNA), and nicking guide RNA (ngRNA). pegRNAs consist of a spacer, single guide RNA (sgRNA) scaffold, reverse-transcriptase template (RTT), and primer binding site (PBS) sequences.

(B) L227R locus with pegRNA+13C>A designs designed to reverse c.680T>G.

(C) DNA correction in 3HA-L227R-CFTR HEK293T cells following plasmid transfection of different pegRNAs and prime editing strategies (PE2 vs. PE3). Tukey's multiple comparisons test did not reveal significant differences between the best-performing +3G>T and +13C>A pegRNAs.

(legend continued on next page)

incidence is reportedly lower but also underdiagnosed and -documented.[8–10] The next challenge is to design efficient therapies for the many (ultra-)rare *CFTR* mutations presenting defects that are not efficiently rescued by HEMTs or that are mechanistically not eligible for HEMTs (i.e., nonsense, splicing, or frameshift mutations).

These mutational classes could be targeted by genetic therapies that either supplement wild-type (WT) *CFTR* nucleic acid sequences or therapies that correct the endogenous alleles. In particular, the implementation of prime editing, a recently developed CRISPR-based system, opens up a new era for treating genetic diseases. The possibility to "rewrite" and correct mutations *in situ* on patients' chromosomes offers therapeutic opportunities for monogenic disorders like CF by preserving endogenous gene expression and regulation, as opposed to gene addition approaches (reviewed in Maule et al.[11]). The prime editor (PE) enzyme leverages the RNA-programmable DNA-targeting ability of *Sp*Cas9 and merges it with RNA-templated, *de novo* DNA synthesis performed by a tethered reverse transcriptase.[12] The template for the reverse transcriptase is provided by a 3′ extension on the CRISPR guide RNA (prime-editing guide RNA [pegRNA]), allowing the programming of the *in-situ*-synthesized DNA strand. The most important advantages of prime editing lie in its capacity to install any nucleotide modification, its inherently high specificity, and its avoidance of double-strand breaks (DSBs). Due to the versatility of the pegRNA design, 97.35% of CF-causing alleles can theoretically be corrected,[2,12] bringing new perspectives for mutations that are too rare to be attractive for classical drug discovery development.

Here, we investigate prime editing for L227R and N1303K, two missense mutations in primary models for CF. L227R is an ultra-rare (29 reported alleles)[2] drug-refractory *CFTR* mutation. With 2,246 reported alleles, N1303K is the fourth most prevalent CF-causing mutation.[2] Of the modulator-ineligible mutations, it is preceded only by G542X, a nonsense mutation leading to premature translation termination.[7] Recent reports, including work from our group,[13,14] show only a modest functional rescue with the most efficient modulator combinations for N1303K, currently excluding it from inclusion in the Trikafta US Food and Drug Administration (FDA) label expansion. L227R leads to an even more severe molecular phenotype and was shown to have no response at all to HEMT.[14] This, together with the severe, pancreatic-insufficient phenotypes, underscores the high unmet medical need of these patient groups.

RESULTS

Prime-editing strategies correct the c.680 T>G (L227R) *CFTR* mutation

To correct L227R at the genomic DNA level, 20 different pegRNAs were designed based on the four closest protospacer adjacent motif (PAM) sites and a matrix of different primer binding site (PBS) and reverse-transcription template (RTT) lengths (Figures 1A, 1B, and S1A). These combinations included high-ranked PBS-RTT lengths designed by available prediction algorithms[15–17] (Table S1). The pegRNAs were tested individually (PE2 approach) as well as in combination with a nicking guide RNA (ngRNA; PE3 strategy) (Figure 1A), as this has been shown to promote incorporation of the installed edit onto the non-edited DNA strand.[12,18] Where possible, PE3b ngRNAs were chosen. These guides contain the target base, i.e., the WT *CFTR* base, in the spacer sequence. Such ngRNAs nick the target sequence only once the pegRNA has completed installation of the desired edit on the opposite strand. The sequential actions of pegRNA and ngRNA lead to increased efficiency and reduced on-target insertion or deletion (indel) formation compared to non-sequential nicking strategies (PE3a).[12] To assess different pegRNA and ngRNA combinations, we transfected guide-encoding plasmids into engineered HEK293T cell lines stably expressing a single integrated pCMV-3HA-L227R-*CFTR* DNA expression cassette. Sanger sequencing and subsequent EditR analysis[19] showed that 12 pegRNAs delivered significant corrections, with the highest levels of correction observed for pegRNA+13C>A (10–19 bp PBS-RTT) (Figures 1C and S1B). Combining pegRNA+13C>A with a PE3b ngRNA (ngRNA-2) led to a mean correction of 25% ± 8% of alleles, corresponding to a 1.6-fold increase in editing compared to the pegRNA alone (Figure 1C). Sanger sequencing was confirmed by next-generation sequencing (NGS) analysis of the same locus (Figures S1C–S1E).

Prime editing of L227R effectively restores CFTR trafficking, glycosylation and function in HEK293T

We found that L227R-CFTR presents with a severe processing defect, as evidenced by the absence of the fully glycosylated Golgi- and post-Golgi fraction (so called mature CFTR, "band C") on western blot and the absence of detectable CFTR at the PM (Figures 1D–1G). Treatment with the optimized PE3 strategy rescued the processing defect of L227R, shown by restoration of band C (Figure 1F). CFTR maturation, calculated as band C/total CFTR relative to the ratio observed in HEK293T-WT-CFTR, was

(D) Percentage of cells with PM-localized CFTR correlates with *CFTR* correction on DNA level. Spearman correlation r = 0.8182, $p < 0.0001$. PM staining and flow cytometry using antibodies against the extracellular 3HA tag of 3HA-L227R-CFTR HEK293T cells.

(E) Percentage of 3HA-L227R-CFTR HEK293T cells positive for PM-CFTR following plasmid transfection of different pegRNAs and prime editing strategies (PE2 vs. PE3).

(F) Western blot of CFTR-negative (NT), control- or L227R PE3-treated 3HA-L227R-CFTR, or wild-type (WT)-CFTR HEK293T cell lines. Bands B and C, respectively, represent core- and complex-glycosylated CFTR.

(G) Immunocytochemistry staining and confocal microscopy of HEK293T NT, control or L227R-targeted 3HA-L227R-CFTR, and 3HA-WT-CFTR cells. DAPI-stained nuclei are represented in blue, and labeling of extracellular 3HA-CFTR is shown in green.

(H) Halide-sensitive yellow fluorescent protein (HS-YFP) quenching assay in NT or L227R- or WT-CFTR HEK293T cells treated with L227R-targeting or control PE3 approaches. Traces and error bars represent $n = 3$ biological repeats.

(I) CFTR function is calculated as $1-F/F_0$ (with F_0 = fluorescence at point of iodide buffer injection) with subtraction of quenching in NT cells (aspecific/background) and relative to WT-CFTR HEK293T cells. Control PE3 = non-*CFTR*-targeting pegRNA + ngRNA (*RNF2* locus). Tukey's multiple comparisons test was used to compare experimental conditions. All data are presented as mean ± S.D. $^*p < 0.05$, $^{**}p < 0.01$, $^{***}p < 0.001$, or $^{****}p < 0.0001$.

42.27% ± 17.4% in the polyclonally edited cell pool (Figure S1F). The 3HA tag positioned in extracellular loop 4 of CFTR in the 3HA-L227R-HEK293T model allows sensitive immunocytochemistry staining of PM-CFTR and was previously shown not to interfere with CFTR trafficking and folding.[20] The recovered CFTR maturation shown on western blot corresponded to the appearance of cells displaying PM-localized 3HA-CFTR on confocal images (Figure 1G). Flow cytometric analysis indicated that 31.07% ± 13.87% of cells were positive for PM-CFTR when treated with PE3 targeting the L227R mutation (Figure 1E). The level of protein rescue (i.e., the percentage of PM-CFTR-positive cells) correlated with DNA correction, suggesting that precise *CFTR* correction led to CFTR maturation and rescue of subcellular localization (Figure 1D, Spearman correlation $r = 0.82$, $p < 0.0001$). Finally, because PM localization is required for, but does not guarantee, proper gating and ion channeling, CFTR function was evaluated through halide-sensitive yellow fluorescent protein (HS-YFP) quenching. Influx of iodide through CFTR leads to rapid quenching of HS-YFP, allowing us to quantify CFTR activity.[20,21] In line with DNA and protein correction levels, use of the optimized PE3 approach showed 24.80% ± 7.74% functional correction relative to WT (Figures 1H and 1I).

Prime-editing strategies correct the c.3909 C>G (N1303K) mutation

To investigate prime editing for N1303K, a second and more common mutation, we designed 16 pegRNAs based on two PAM sites and 4 different ngRNAs (Figure S2A). Two of these ngRNAs (ngRNA-1, ngRNA-2) classify as PE3b ngRNAs and the remaining as PE3a strategies.[12] Analogous to our approach for L227R, we tested different pegRNA-ngRNA combinations in a 3HA-N1303K-CFTR HEK293T stable cell line. Of these, pegRNA+13C>G (14–18 bp PBS-RTT) induced editing levels up to 27.3%± 4.2% when combined with ngRNA-1 (Figures 2A and S2B–S2D). Of note, the PE3b approach using ngRNA-1 on average increased PE efficiencies 3.17-fold compared to the respective pegRNA alone (Figure S2E). The other ngRNAs did not significantly increase correction. ngRNA-1 positions the C>G correction in the PAM-proximal region (seed region) of its spacer, in contrast to ngRNA-2, where the desired edit is part of the PAM-distal spacer region (non-seed).

Prime editing of N1303K effectively restores CFTR trafficking, glycosylation, and function

N1303K is traditionally classified as a class II processing mutant, although we and others have reported an additional severe gating defect.[13,22–24] HEK293T cells overexpressing 3HA-N1303K-CFTR recapitulate these phenotypes[13] and allow us to investigate in a first step whether prime editing can correct these known molecular defects. At baseline, western blot and extracellular labeling of CFTR show small amounts of complex glycosylated CFTR (band C) and limited PM localization but no residual ion channel function as measured by HS-YFP quenching (Figures 2B–2E). Treatment with the optimized PE3 combination resulted in a substantial increase in mature CFTR (50.30% ± 15.46% band C/total CFTR relative to HEK293T-WT-CFTR cells), whereas such rescue was not obtained with the triple modulator combination (elexa-, teza-, ivacaftor [ETI]) (Figures 2B and S2F). Similarly, staining against the extracellular 3HA tag indicated substantial rescue of 3HA-N1303K-CFTR trafficking by prime editing. This was evidenced by cells presenting with a high, WT-like CFTR PM density on confocal microscopy (Figure 2C) and quantified by flow cytometry, resulting in 30.5% ± 3.7% of gene corrected, $CFTR^{high+}$ cells (Figures 2D and S2H). Lastly, CFTR function was also rescued, resulting in 22.47% ± 5.54% HS-YFP quenching relative to WT-CFTR (Figures 2E and S2I).

Improving prime-editing efficiency by enhanced pegRNA and prime-editing designs

Because PE activity requires an intact PBS to prime the tethered RT, outcome efficiency can be critically hampered by the degradation of the unprotected 3′ ends of pegRNAs by intracellular exonucleases.[25] We evaluated whether the addition of a 3′ "capping" motif[25] could increase our editing levels. For both mutations, such engineered pegRNAs (epegRNAs; 3′ tevopreQ1-motif) outperformed the original pegRNAs, leading to 21.0% ± 6.5% editing for L227R and 43.3% ± 10% editing for N1303K, corresponding to 1.49- and 1.33-fold increases, respectively (Figure S3A).

Because PE achieves gene correction through a three-DNA-strand intermediate, modulation of DNA mismatch repair (MMR) can be used to beneficially impact prime-editing outcomes.[26,27] For N1303K, we investigated the addition of three extra synonymous MMR-evading mutations. Sequencing chromatograms showed efficient installation of the additional silent mutations, but overall editing efficiency in this model was not increased (Figures S3B and S3D). For L227R, we introduced a silent PAM-disrupting mutation but also here no increase in editing efficiency was observed (Figures S3B and S3C). Lastly, we also evaluated the PE5max system,[26] which leverages a dominant-negative MLH1 (MLH1dn) to suppress MMR activity together with an optimized PE-enzyme (PEmax). MLH1 is a key effector of the MMR pathway, which has been shown to negatively impact the prime-editing outcomes.[27,28] In HEK293T, the use of PE5max resulted in similar efficiencies to PE3 in the same model (Figure S3E).

Prime editing of the endogenous *CFTR* locus in rectal organoids derived from pwCF restores CFTR function

To validate our prime editing approach, we transitioned to primary cells from CF donors. Rectal organoids have been established as a highly translational model for CFTR function and allow to reliably predict the efficacy of therapeutic strategies.[29] CFTR activation through the addition of forskolin leads to rapid volumetric expansion of these organoids[30] (forskolin-induced swelling [FIS], Figure 3A), providing a functional platform to study *CFTR* gene correction.[31–34] For CFTR modulators, FIS responses correlate with non-gastrointestinal clinical endpoints in pwCF, including lung function.[35,36] Upon treatment of L227R organoids with ETI, no improvement in CFTR function was detected, underscoring its drug-refractory nature (Figures S4A and S4B). N1303K showed a moderate response to ETI, as reported before[13] (Figures S4A and S4B).

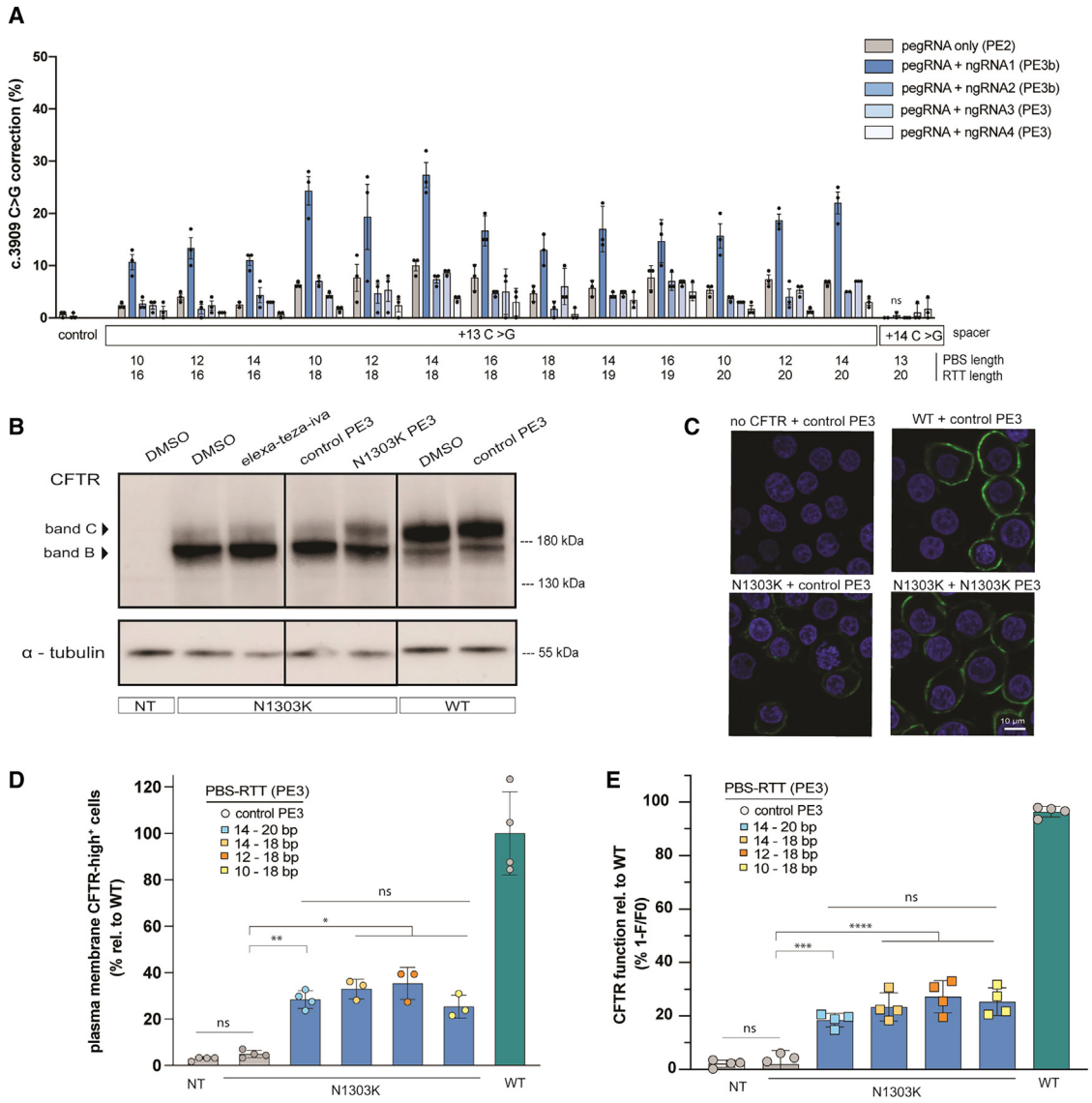

Figure 2. Prime editing of c.3909C>G (N1303K) rescues CFTR glycosylation, PM localization, and channel function

(A) DNA correction in 3HA-N1303K-CFTR HEK293T cells following plasmid transfection of different pegRNAs and prime-editing strategies (PE2 vs. PE3).

(B) Western blot of CFTR-negative (NT), 3HA-N1303K-CFTR, or WT-CFTR HEK293T cell lines treated with control PE3, N1303K PE3, elexa-teza-ivacaftor (ETI; 3 μM of each, 24 h incubation), or DMSO control. Bands B and C respectively represent core- and complex-glycosylated CFTR.

(C) Immunocytochemistry staining and confocal microscopy of HEK293T NT, 3HA-WT-CFTR, and control- or N1303K-PE3-treated 3HA-N1303K-CFTR cells. DAPI-stained nuclei are represented in blue, and labeling of extracellular 3HA-CFTR is shown in green.

(D) Percentage of PM-CFTR^{high+} PE3-treated 3HA-N1303K-CFTR cells relative to WT. High^{+} cells were gated based on non-treated 3HA-N1303K HEK293T cells. Gating strategy is shown in Figure S2H.

(E) HS-YFP quenching assay of control- or N1303K PE3-treated HEK293T expressing no CFTR (NT), N1303K-CFTR, or WT-CFTR. CFTR function is calculated as 1-F/F_0 (with F_0 = fluorescence at point of iodide buffer injection) with subtraction of quenching in NT cells (aspecific/background) and relative to WT-CFTR HEK293T cells. Control PE3 = delivery of non-*CFTR*-targeting pegRNA + ngRNA (*RNF2* locus). All data points reflect biological replicates, presented as mean ± SD. Tukey's multiple comparisons test was used to compare experimental conditions. *$p < 0.05$, **$p < 0.01$, ***$p < 0.001$, or ****$p < 0.0001$.

To evaluate prime editing efficiency in pwCF-derived rectal organoids, we delivered PE together with optimized pegRNAs and ngRNAs via lentiviral vectors (LVs). For both genotypes (homozygous and compound heterozygous samples), treatment with mutation-specific pegRNAs led to the growth of organoids with a clear lumen and swelling after forskolin stimulation (Figure 3B), underlining that also in primary cells, prime editing restores CFTR function. Analysis of the L227R- and N1303K-encoding loci indicated efficient and precise introduction of the nucleotide substitutions (Figures S4C and S4D). Although prime editing was overall accurate, deep sequencing (>2 million reads/amplicon) uncovered infrequent undesired

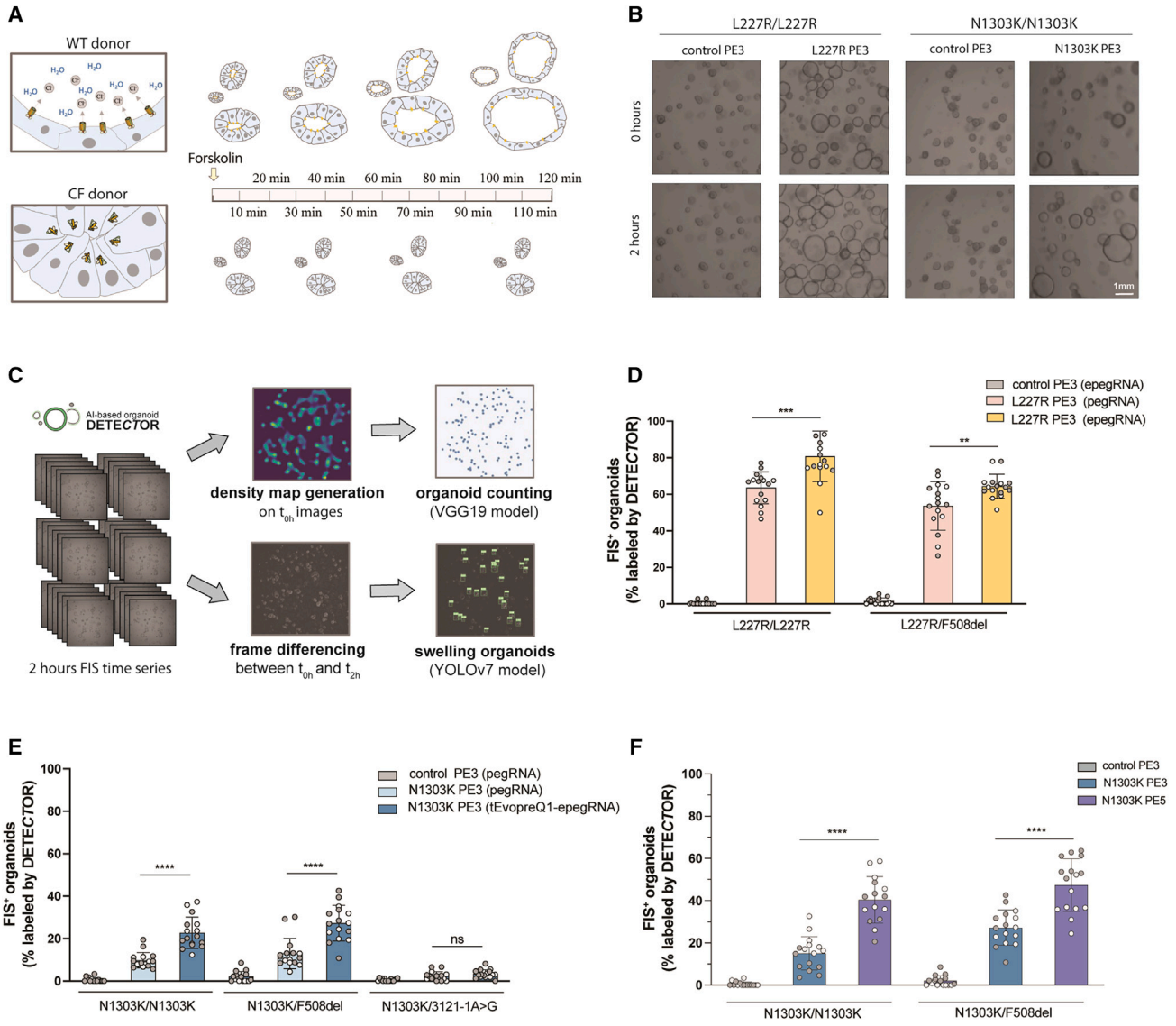

Figure 3. Prime editing of the endogenous *CFTR* locus restores CFTR function in patient-derived rectal organoids

(A) Forskolin-induced swelling (FIS) in rectal organoids is a CFTR-dependent/-specific phenotype and hence well suited to evaluate functional correction after prime editing.

(B) Representative images from FIS experiments in organoids homozygous for L227R or N1303K transduced with lentiviral vectors (LVs) encoding PE enzyme, pegRNA, and ngRNA.

(C) To assess individual organoid swelling, a machine learning-based algorithm was developed: DETECTOR (detection of targeted editing of *CFTR* in organoids). The tool first counts all organoids and subsequently evaluates the number of swelling organoids based on an image that overlays individual organoid areas at the start and end of the FIS assay (difference image).

(D) Percentage of FIS-responsive organoids (determined by DETECTOR) in samples from patients homozygous or heterozygous for L227R treated by LV-delivered PE3 approaches. Unpaired parametrical t test with Welch's correction was used to compare groups.

(E) Percentage of FIS-responsive organoids (determined by DETECTOR) in samples from patients homozygous or heterozygous for N1303K. Mann-Whitney U t test was used to compare groups.

(F) Percentage of FIS-responsive organoids following co-transduction of LVs containing PE, pegRNA, and ngRNA with an LV expressing MLH1dn (PE5 strategy) in organoids homozygous or heterozygous for N1303K. Unpaired parametrical t test was used to compare groups. Bars represent the mean of two biological replicates measured as technical octuplicates. Control PE3 = delivery of non-*CFTR*-targeting PE3 approach (*RNF2* locus). $^{*}p < 0.05$, $^{**}p < 0.01$, $^{***}p < 0.001$, or $^{****}p < 0.0001$.

alleles (indels) in some of the most efficiently edited samples (Figures S4E and S4F).

ML-based detection to precisely determine functional correction in organoids

Quantification of the organoid response to CFTR modulators in the FIS assay is typically based on the increase in total organoid surface area measured over a fixed period of time.[30,37] This is a valid approach since responses to small molecules are relatively homogeneous. For gene editing approaches, however, responses of individual organoids are binary (CF or WT phenotype). Hence, increases in total organoid surface are less informative and easily biased by the size of (un) responsive organoids (Figures S4G and S4H). To circumvent arduous manual inspection and quantification, we developed a software tool that allows automated and label-free analysis of the effect of genetic therapies based on individual organoid phenotype. DETECTOR (detection of targeted editing of *CFTR* in organoids) is a machine learning (ML)-based image processing algorithm capable of analyzing dynamic, large-scale, bright-field microscopy data (Figure 3C). DETECTOR employs two parallel ML models to first count and subsequently evaluate swelling in individual organoids (Figures S4I and S5A). The counting and swelling models were trained on 18.499 and 4.093 labeled structures, respectively, and achieved 94% (MAE = 5.20%, MSE = 6.31%) and 85% (AP_{50} = 0.85) accuracy compared to manual analysis. To validate the model further, N1303K homozygous organoids were pre-treated with ETI and stimulated with 5 μM forskolin, a therapy that should lead to detectable swelling in all organoids. DETECTOR flagged 103% ± 13% as positive, while 0% ± 0% swelling organoids were detected in the DMSO control (Figure S5B). Note that DETECTOR flags all organoids with any swelling phenotype regardless of their relative size increase. Consequently, DETECTOR is well fit for the evaluation of gene editing outcomes but not for continuous modulator responses.

MMR modulation enhances prime-editing outcomes in patient-derived rectal organoids

Next, we leveraged DETECTOR to functionally dissect different prime editing approaches in primary cells harboring one or two L227R or N1303K alleles (Figures 3D and 3E). The L227R-targeting PE3b approach (PE + pegRNA + ngRNA) compared to PE2 (PE + pegRNA) delivered a 4.99-fold increase in swelling of L227R homozygous organoids (Figure S5C). Use of the evopreQ1-epegRNA architecture combined with PE3b further increased the frequency of phenotype-corrected organoids up to 80.0% ± 13.8% for L227R and 27.3% ± 8.3% for N1303K organoids (Figures 3D and 3E). Consistent with results in HEK293T, the introduction of a synonymous PAM disruption mutation for L227R did not increase the number of FIS-responsive organoids (Figure S5D).

Since primary organoids are MMR proficient (Figure S5E), both MMR-evading epegRNA designs as well as PE4/PE5 approaches were investigated. Interestingly, epegRNAs encoding additional silent edits, alongside the desired N1303K correction, improved editing in a PE2, but not a PE4, setup (Figure S5F). In quadruple transduction experiments using an additional LV expressing MLH1dn (PE + epegRNA + ngRNA + MLH1dn), DETECTOR recorded an average 2.16-fold increase in functional correction compared to the triple transduction PE3b condition, leading to 45.7% ± 15.1% of functionally corrected organoids (Figure 3F). Use of PEmax instead of the PE2 enzyme did not further increase editing efficiencies (Figure S5G).

Measuring the same organoids in a second FIS assay 1 week after the first (i.e., 3 weeks post-transduction) showed that the functional correction is durable, in contrast to modulator-induced responses (Figure S5H). When combining data from all evaluated PE systems (i.e., PE2-PE3b-PE4-PE5, PEmax, pegRNA-epegRNA, MMR-evading silent edits), the functional response reported by DETECTOR correlated with the observed percentages of DNA correction (Figure S5I, Pearson r = 0.78, $p < 0.0001$, for L227R).

Prime editing of the endogenous *CFTR* locus restores CFTR function in patient-derived airway epithelia

Although CF is a systemic disease, morbidity and mortality mainly stem from lung pathology, and hence the airway epithelium is currently the primary target for CF gene replacement or gene editing therapy. To evaluate whether prime editing would also allow us to functionally correct *CFTR* mutations in the airway epithelium, we engineered the parental 16HBE14o- (human bronchial epithelial) cell line, as well as 16HBEgeN1303K that contains the mutation in the endogenous *CFTR* gene,[38] to express a single integrated HS-YFP cassette (Figure S6A). Upon LV-mediated delivery of the optimized PE3max approach, 23.68% ± 2.31% *CFTR* DNA correction was detected in 16HBEgeN1303K-YFP and 37.33% ± 6.35% in 16HBEgeN1303K-MLH1dn-YFP (Figure 4A). These editing levels corresponded to 10.8% ± 0.2% and 20.3% ± 4.3% HS-YFP quenching relative to WT (Figures 4A and S6B). The difference observed in DNA editing and functional rescue can be attributed to the fact that 16HBEgeN1303K is homozygous for the N1303K mutation but only possesses one functional *CFTR* allele.[38,39] Next, we delivered all three PE components to patient-derived human nasal epithelial (HNE) basal cells with L227R/L227R, N1303K/R1162X, N1303K/N1303K, or WT genotypes through LV delivery. HNEs were differentiated at the air-liquid interface (ALI) and functionally evaluated through Ussing chamber short-circuit current measurements 4 weeks post-transduction (Figures 4B–4E, S6C–S6G, S7A, and S7B). PE3-treated L227R cultures displayed forskolin-induced currents of 13.3 ± 2.6 μA/cm^2 (Figure 4D) that were completely inhibited by Inh172 (14.0 ± 4.1 μA/cm^2), a specific CFTR inhibitor. PE3-treated N1303K cultures showed a CFTR functional rescue, albeit modest at 1.03 ± 0.32 μA/cm^2 (Figure 4E). The CFTR currents measured in prime edited epithelia derived from L227R and N1303K donor samples, respectively, corresponded to 29.4% and 2.3% relative to the average currents measured in cells derived from WT donors. In these experiments, PE5 did not significantly increase functional rescue. Interestingly, the highest levels of genomic HNE correction that we could detect were 1.27% ± 0.29% and 0.57% ± 0.56% for L227R and N1303K, respectively (Figures S7C–S7E). A clear correlation was observed between genomic

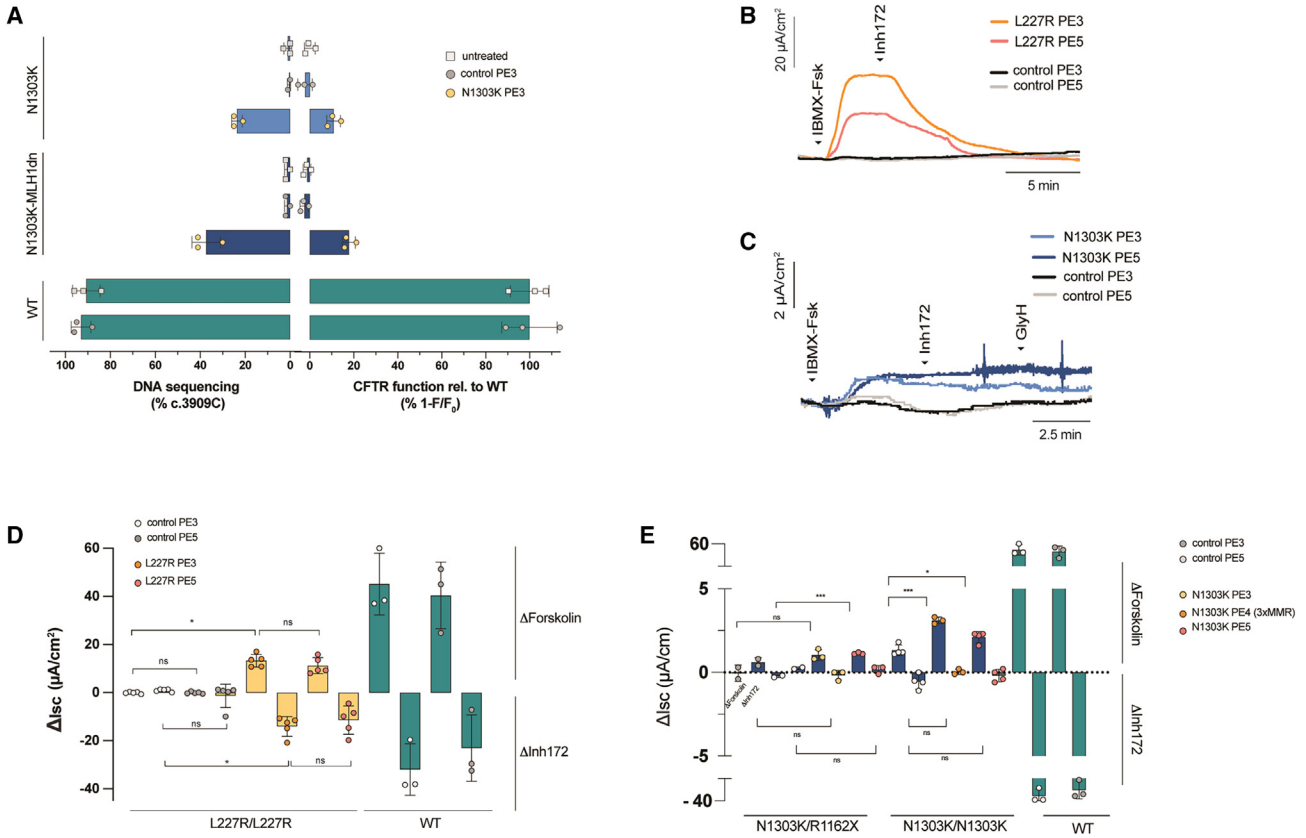

Figure 4. Prime editing of the endogenous *CFTR* locus restores CFTR function in 16HBE and primary nasal epithelial cells

(A) DNA correction and correction of CFTR function in engineered 16HBEgeN1303K-YFP and 16HBEgeN1303K_MLH1dn-YFP cells transduced with LVs encoding PE enzyme, engineered pegRNA (epegRNA), and ngRNA. CFTR function was determined by HS-YFP quenching and calculated as 1-F/F_0 (with F_0 = fluorescence at point of iodide buffer injection) relative to WT 16HBE-YFP cells.

(B and C) Representative short-circuit currents (Isc) of human nasal epithelial (HNE) cells with L227R/L227R (B) or N1303K/R1162X (C) genotypes. HNEs were transduced with LVs containing PE3 or PE5 components and subsequently differentiated at the air-liquid interface (ALI). Arrows indicate the addition of 100 μM 3-isobutyl-1-methylxanthine (IBMX) + 10 μM forskolin (Fsk) or 10 μM Inh172.

(D and E) Quantified CFTR-dependent Isc (ΔFsk/IBMX and ΔInh172) for PE3 or PE5 of (D) L227R homozygous and WT HNEs and (E) N1303K/N1303K, N1303K/G1182X, and WT HNEs. Bars represent $n = 5$ or $n = 3$ biological repeats, and error bars represent SD. WT HNEs are the same in (D) and (E). Tukey's multiple comparisons test was used to compare experimental conditions. Control PE3/PE5 = delivery of non-*CFTR*-targeting pegRNA + ngRNA (*RNF2* locus).

and functional correction of the cultures that responded to the prime editing therapy (r = 0.93, $p = 0.003$; Figure S7F).

Prime editing corrects CF-causing mutations with high fidelity

To verify the specificity of the optimized epegRNAs and ngRNAs for L227R and N1303K, we used computational as well as experimental methods to identify genomic sites with increased propensity for off-target (OT) *Sp*Cas9 binding and editing. First, we used CRISPOR[40] to predict and rank potential OT sites based on their cutting frequency determination score[41] (Table S4). Next, to experimentally identify sites prone to *Sp*Cas9-dependent aspecific activity, we performed an unbiased whole-genome OT analysis method, GUIDE-seq (GS),[42] in HEK293T cells with catalytically active *Sp*Cas9 nuclease. For L227R, three and nine OT sites were identified by GS for the optimized epegRNA and ngRNA, respectively (Figure 5A; Table S4). For N1303K, one and three OT sites were detected for the optimized epegRNA and ngRNA, respectively (Figure 5B; Table S4). Multiple OT sites found via GS were also among those flagged by CRISPOR. We selected all OT sites identified through GS, as well as the highest ranked CRISPOR OTs, for further in-depth genetic analysis in HEK293T cells treated with PE3. Targeted deep sequencing on these sites in PE-treated HEK293T-L227R/N1303K-CFTR cells showed no editing at the expected nick sites in L227R/N1303K PE3 or control samples (Figures 5C and 5D). On the position of the PE-encoded edit, no significant events were detected at any of the OT sites, whereas clear introduction of the correction was found at the intended target sites within *CFTR* (Figures S8A–S8D).

Because prime editing and hence also potential OT prime editing can be affected by cell-specific expression of DNA damage repair (DDR) machinery, we repeated deep sequencing in organoid samples that displayed high functional correction (Figures 5C and 5D). Again, we found no evidence of PE activity at the investigated sites.

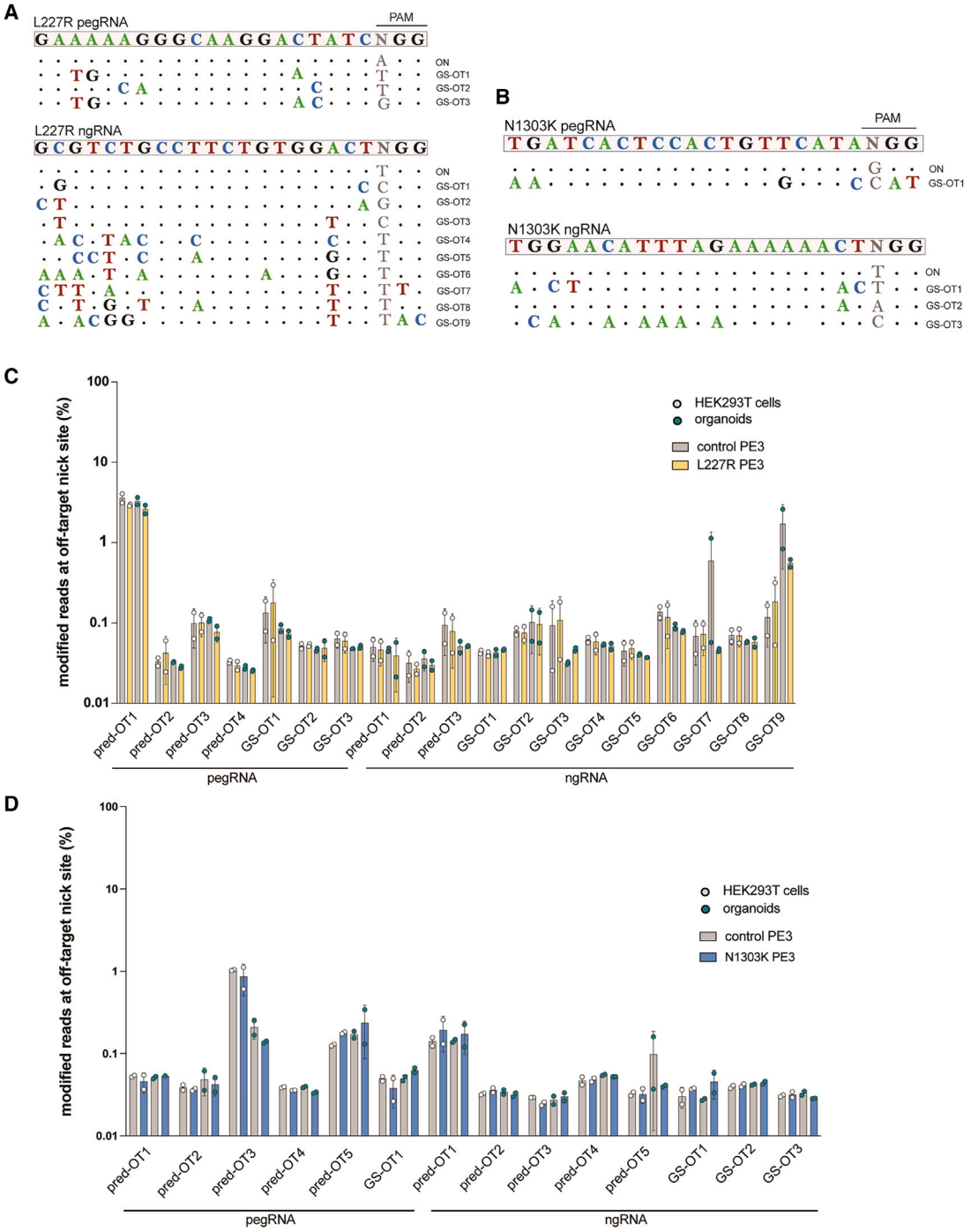

Figure 5. Off-target profiling of L227R and N1303K prime-editing guides

(A and B) Potential *Sp*Cas9 off-target sites identified through GUIDE-seq in HEK293T cells using *Sp*Cas9 combined with (A) L227R and (B) N1303K pegRNAs and ngRNAs.

(C and D) Targeted deep sequencing on potential off-target sites identified by *in silico* prediction and/or GUIDE-seq. HEK293T samples were collected 3 days after transfection. Organoid samples were harvested 14 days post-transduction. Bars represent mean percentage of modified reads evaluated at expected nick site ± SD of two biological replicates. Control PE3/PE5 = delivery of non-*CFTR*-targeting pegRNA + ngRNA (*RNF2* locus).

DISCUSSION

Considering the monogenic and serious nature of CF, *CFTR* was among the first targets to be investigated for therapeutic correction by canonical *Sp*Cas9 editing and subsequent homology-directed repair (HDR). In initial studies, editing efficiencies were too low for clinical application,[43,44] but recently, editing efficiencies >40% have been achieved and can be further increased by *ex vivo* enrichment of edited cells.[45,46] However, Cas9/HDR approaches are critically cell-cycle dependent, limiting the *in vivo* application of this approach. Furthermore, they require the introduction of a DSB, an event that can lead to genotoxicity.[47–50] Aside from HDR strategies which can theoretically be applied to any given mutation, targeted CRISPR-Cas approaches were previously limited to two subsets of mutations: intronic splicing mutations that can be disrupted using cleaving Cas orthologs and nonsense or canonical splice site mutations that can be more precisely reverted by base editing,[51] together covering ~1/3 of known CF-causing variants (32.26%).[2]

Prime editing, on the other hand, is theoretically capable of correcting all base conversions and small indels, covering 97.35% of all CF-causing variants.[2,12] In our study, we report on the successful prime editing of the L227R and N1303K mutations. Both lead to severe CFTR defects, are currently ineligible for available modulators, and are caused by base transitions that cannot be corrected using base editing or DSB approaches without HDR. We optimized pegRNA design in HEK293T cells stably expressing 3HA-L227R/N1303K-*CFTR* and showed that DNA correction of either mutation led to restored protein glycosylation, PM localization, and function.

It is, however, important to recognize that PE is not a standalone effector: PE merely installs a complex three-strand DNA intermediate that ought to be resolved by target cell DDR machinery. Consequently, prime editing is critically dependent on the expression and activity of several host factors.[25–27,52] HEK293T cells are a straightforward model to investigate the functionality of different pegRNA designs[18] and prime editing strategies, but they might not accurately represent the expression and organization of PE-impacting host factors found in primary cells. To validate prime editing in a more translational model, PE and guideRNAs were delivered to rectal organoids derived from pwCF. These organoids are a well-established model in the CF field, shown to robustly predict patient responses to CFTR-targeting therapies.[29,36] Prime editing in intestinal organoids has been previously reported by Geurts et al. and Schene et al. but required clonal outgrowth and/or selection to detect DNA correction.[53,54] In our work, through pegRNA design optimization in HEK293T cells, careful dissection of recent prime editing innovations, and LV-mediated delivery into primary cell models, we achieved up to 34% genomic *CFTR* correction resulting in up to 80% functionally rescued organoids. The correction levels were measured 2 weeks after a single treatment and without any form of selection.

Next, the developed prime-editing strategies were also delivered to 16HBE and pwCF-derived HNE airway epithelial cells. In both models, genetic correction led to significant correction of CFTR function. In 16HBEgeN1303K expressing HS-YFP, a quenching of 20.3% ± 4.3% relative to WT was observed for N1303K. In ALI-differentiated HNE from pwCF, short-circuit current measurements detected 2.3% and 29.4% functional correction (relative to WT) for N1303K and L227R, respectively. Previous studies with modulators on pwCF-derived HNE predicted that currents as low as 5%–10% of WT are sufficient to deliver clinical improvements measured as forced expiratory volume in 1 s.[55–58] In differentiated epithelial cells homozygous for L227R, the meaningful correction (~30% of WT) was caused by only 1.27% ± 0.29% of precise gene editing. These data thereby suggest that correction of *CFTR* in only a small percentage of airway epithelial cells can lead to a meaningful increase in CFTR function, a promising indication for future CF genetic therapies.

Because validation of prime editing in primary, pwCF-specific models is crucial to understand its impact toward clinical translation, we set out to develop a computational tool for functional organoid gene editing analysis. Following the increasing use and relevance of organoids in medical research, multiple analysis tools have been developed.[59–62] These tools are, however, not equipped to analyze swelling of individual organoids specifically. We therefore developed DETECTOR, an ML-based algorithm. DETECTOR detects organoids that gain the typical CFTR-dependent lumen formation and swelling and applies a binary label (swelling or non-swelling). Unlike regular surface-based FIS analysis, DETECTOR is not critically dependent on an increase in organoid surface area and is hence able to handle pre-swelling that may arise from early gene correction and restored endogenous CFTR function. DETECTOR was also trained to detect organoids that expand little in size but clearly obtain a lumen, rendering it a useful tool for evaluating *CFTR* gene editing or other *CFTR*-targeting therapies. Although HEK is still the preferred model for setting up prime-editing strategies, screening in primary models might ultimately be more relevant, and AI-based tools such as DETECTOR can support these efforts in a non-biased, standardized, rapid, and scalable manner. In fact, we observed that L227R was less efficiently corrected in the HEK293T-L227R-CFTR model (21.0% ± 6.5% for epegRNA-based PE3) compared to the >40% correction efficiency for N1303K-CFTR in the same cell model. Conversely, L227R was more efficiently corrected and rescued in primary rectal organoids and HNE cultures from different donors, whereas N1303K was only moderately corrected. The same observations were made in the primary HNE model, further evidencing the importance of screening in primary, translational models.

For the most efficient epegRNAs and ngRNAs, we investigated the safety profile of our PE approaches through *in silico* prediction and experimental identification of potential OT sites. GUIDE-seq analysis identified several sites prone to OT Cas9 binding and cleavage. Deep sequencing analysis of PE-treated HEK293T cells at these sites could not reveal any significant PE activity. Also in patient-derived organoids, no OT activity was detected, underscoring previously reported PE safety and fidelity.[12,53,63–65] Neither plasmid transfection nor triple/quadruple LV transduction are translational delivery strategies, yet they allow us to investigate whether precise gene correction is possible and whether this can rescue CFTR function. Moreover, transduction with LVs driving high-expression cassettes for PE effectors and guides, together with a stable, 2-week

exposure, allows us to probe for the specificity of the system, since prolonged exposure is one of the main drivers behind OT activity.[66] The fact that none can be found after 2 weeks of high expression further adds to the already well-documented safety profile of PE.[12,53,63–65]

For severe monogenic disorders caused by relatively common mutations, such as sickle cell disease or common *CFTR* mutations, the investment in innovative approaches by the pharma industry is obvious or already present.[67] Providing proof-of-principle data on common *CFTR* variants, such as F508del (first)[51] or N1303K (fourth), the latter exemplified in this study, is therefore important. However, identifying strategies to tackle rare variants might be even more impactful, as, worldwide, hundreds of millions of patients suffer from disorders caused by rare variants.[68] This population includes pwCF with genotypes non-responsive to HEMTs, most of which are rare to ultra-rare (<1%), such as the L227R mutation characterized and tackled in this work. Importantly, these patient groups do not allow for classical clinical trial designs due to the small number of patients for each mutation, urging for alternative trial designs and new criteria for proving efficacy.[69]

CRISPR medicines are especially attractive for such rare mutations since, once safe and efficient delivery has been established, only the respective guide RNAs must be switched and evaluated. In fact, one or multiple strategies have already been reported for many of the most common *CFTR* mutations (listed in Bulcaen and Carlon[51]). One might envision personalized gene editing pipelines with target-specific guide RNAs to be designed *in silico* and subjected to automated efficacy and safety analysis using relevant primary models.[70] Such gene therapies could be administered to patients in "n-of-1/low patient numbers" clinical trials.[70] Development of better *in silico* pegRNA prediction tools further supports such a model by reducing the number of guides requiring experimental testing.[15–17] Notably, since PE rewrites an entire stretch of DNA, a single pegRNA could be used to correct multiple mutations found within the same locus. In fact, the RTT of our L227R and N1303K pegRNAs, for instance, also spans c. 695T>A (V232D) and c.3908del (N1303TfsX25), two other CF-causing variants. Recent PE-derived approaches such as TwinPE and PASTE allow to write or land longer stretches of DNA, extending the use of PE for correcting entire exons or landing a super-exon with a single pair of pegRNAs.[71,72]

CF modulators already have been paving the road toward an *ex-vivo*-based approval of therapeutics with a known in-man safety profile: in 2017, the FDA granted a label extension for Kalydeco and in 2020 for Symdeko and Trikafta based on pre-clinical data from Fisher Rat Thyroid cells overexpressing CFTR variants to guide its decision.[73,74] Likewise, in Europe, a regulatory pathway has been proposed to leverage the strong correlation between CF organoid and individual patient responses[37,75] (reviewed in Mayer-Hamblett et al.[69]). Individuals with rare *CFTR* mutations exceeding an *a priori* response to candidate drugs could then progress to an n-of-1 trial using their own biological materials. These examples not only offer a potential path for regulatory approval for specific *CFTR* mutations but also represent a precision-based therapy approach toward personalized medicine for CF and beyond.

In conclusion, in this study, we took a step toward a personalized medicine approach by precise gene editing for two CF-causing variants, an ultra-rare (L227R) as well as a more prevalent (N1303K) *CFTR* mutation. We showed that screening of pegRNA and ngRNA configurations in HEK293T cells allowed us to identify functional guide designs and combinations for efficient correction of the *CFTR* gene, CFTR glycosylation, PM localization, and function. Importantly, substantial functional correction was obtained in patient-derived rectal organoids and primary AIL cultured HNE cells. With the development of DETECTOR, an ML algorithm amenable to high-throughput analysis of CFTR functionally corrected organoids, we provide tools for automated screening for genetic strategies to tackle rare CF mutations. Extensive on-target and OT profiling underscores that PE presents high-precision, high-fidelity gene correction even following prolonged and high exposure. In addition, we show that genomic correction levels as low as 1.5% in differentiated primary airway epithelia were sufficient to rescue CFTR chloride currents, further highlighting the potential of gene and prime editing for further investigation toward in-patient testing once optimal delivery vehicles are identified that can circumvent the known CF lung barriers.[76]

Limitations of the study

The current study provides proof of principle for prime editing as a therapeutic strategy for CF but does not tackle the delivery challenge. The human lung naturally presents with several significant barriers that impede straightforward delivery, and the CF lung even more so.[76] In this study, triple or quadruple LVs were used to administer the gene editing cargo to primary cells, a strategy incompatible with therapeutic in-patient gene editing. We evaluated genetic and functional correction in four different models with increasing translatability. In HEK293T-CFTR-overexpressing cells, the level of genetic rescue furthermore correlated well with the level of CFTR protein rescue at the PM, supporting precise gene editing. In primary cell models, however, reliable detection of endogenous CFTR protein expression poses a challenge[77] and hence was not performed in this study. Therefore, at this point, an outstanding question is which exact cell types in a differentiated airway epithelium contributed to the functional correction observed. Finally, we delivered the gene editing machinery to progenitor cell populations before proliferation and differentiation. Future work should thus focus on (1) elucidating the ideal target cell type(s) for therapeutic CF gene editing and (2) combining the developed prime editing approaches with clinically compatible delivery vehicles on fully differentiated airway epithelia, encompassing the apical and basolateral barriers, as they are present in the CF lung.

STAR★METHODS

Detailed methods are provided in the online version of this paper and include the following:

- KEY RESOURCES TABLE
- RESOURCE AVAILABILITY
  - Lead contact
  - Materials availability
  - Data and code availability

SUPPLEMENTAL INFORMATION

Supplemental information can be found online at https://doi.org/10.1016/j.xcrm.2024.101544.

ACKNOWLEDGMENTS

We thank Liesbeth De Keersmaecker for excellent technical support. We acknowledge the Leuven Viral Vector Core for viral vector production. We thank Tine Bulcaen for the design of the DETECTOR logo. Images were recorded on a Zeiss LSM 880 - Airyscan (Cell and Tissue Imaging Cluster), supported by Hercules AKUL/15/37_GOH1816N and FWO G.0929.15 to Pieter Vanden Berghe, University of Leuven. We acknowledge Gergely Lukacs for the 3HA-CFTR constructs and Luis Galietta for HS-EYFP (F46L-H148Q-I152L). We thank the Genomics Core, a KU Leuven Core facility, for performing sample prep and Illumina Novaseq NGS. The computing resources and services used in this work were provided by the VSC (Flemish Supercomputer Center), funded by the Research Foundation - Flanders (FWO) and the Flemish government. This research was funded by grants from the Mucovereniging Belgium and Fund Alphonse Jean Forton from the King Baudouin Foundation (2020-J1810150-E015), Emily's Entourage (US_172749169_6), Research Foundation - Flanders (FWO) (SBO OrganID; S001221N), and KU Leuven Internal Funds C2 (C24M/21/041). M.B. and M.M.E. were supported by FWO-SB doctoral fellowships 1SE8122N and 1S29917N, respectively. Work done by G.M. and A.C. was supported by the Italian Cystic Foundation FFC#2/2021 and M.C. by the Horizon Europe EIC Pathfinder program AAVolution (grant agreement 01071041). Work done by E.D., M.K., A.H., and B.C. was supported by Vaincre La Mucoviscidose (RC20210902984and RC20220503011), Mucoviscidose ABCF2. M.S.C. previously was a senior post-doctoral FWO scholar (12Z5920N) and is now supported by a KU Leuven BOFZAP professorship.

AUTHOR CONTRIBUTIONS

M.S.C. and M.B. designed the research. M.B. performed the experiments, analyzed the data, and wrote the manuscript. M.B. and R.B.L. developed the ML models to analyze organoid responses. M.B., P.K., S.T., and M.M.E. performed experiments in human cell lines and analyzed data. G.M. and M.C. performed GS experiments and analyzed the results. M.B. analyzed GS and NGS data. E.D., M.K., and M.B. performed Ussing chamber experiments in primary HNE cells. M.B., S.T., and A.S.R. performed organoid experiments and analyzed data. M.S. produced the LVs through the Leuven Viral Vector Core under the supervision of R.G. Principal investigators X.C.i.S., F.V., Z.D., R.G., I.S.-G., and A.C. supervised the research. M.S.C. supervised the research and wrote the manuscript. All authors read and approved the final manuscript.

DECLARATION OF INTERESTS

A.C. is a co-founder and holds shares of Alia Therapeutics. I.S.-G. is scientific board adviser of, received academic grants from, and supervises a study sponsored by Vertex Pharmaceuticals. I.S.-G. is a scientific board adviser of Tavanta. M.S.C. received speaker fees from Vertex Pharmaceuticals.

Received: July 26, 2023
Revised: January 16, 2024
Accepted: April 10, 2024
Published: May 1, 2024

REFERENCES

1. Guo, J., Garratt, A., and Hill, A. (2022). Worldwide rates of diagnosis and effective treatment for cystic fibrosis. J. Cyst. Fibros. *21*, 456–462. https://doi.org/10.1016/j.jcf.2022.01.009.
2. Cystic Fibrosis Foundation (CFF) (2023). CFTR2 Variant List History. https://cftr2.org/mutations_history.
3. Cutting, G.R. (2015). Cystic fibrosis genetics: From molecular understanding to clinical application. Nat. Rev. Genet. *16*, 45–56. https://doi.org/10.1038/nrg3849.
4. Rommens, J.M., Iannuzzi, M.C., Kerem, B., Drumm, M.L., Melmer, G., Dean, M., Rozmahel, R., Cole, J.L., Kennedy, D., Hidaka, N., et al. (1989). Identification of the cystic fibrosis gene: Chromosome Walking and Jumping. Br. Med. J. *245*, 1059–1065. https://doi.org/10.1136/bmj.300.6733.1198-a.
5. Kerem, B.-S., Rommens, J.M., Buchanan, J.A., Markiewicz, D., Cox, T.K., Chakravarti, A., Buchwald, M., and Tsui, L.-C. (1989). Identification of the cystic fibrosis gene: genetic analysis. Trends Genet. *5*, 363. https://doi.org/10.1016/0168-9525(89)90156-X.
6. Riordan, J.R., Rommens, J.M., Kerem, B.-S., Alon, N., Rozmahel, R., Grzelczak, Z., Zielenski, J., Lok, S., Plavsic, N., Chou, J.-L., et al. (1989). Identification of the cystic fibrosis gene: Cloning and characterization of complementary DNA. Trends Genet. *5*, 363. https://doi.org/10.1016/0168-9525(89)90155-8.
7. Ensinck, M.M., and Carlon, M.S. (2022). One Size Does Not Fit All: The Past, Present and Future of CF Causal Therapies. Cells *11*, 1–44. https://doi.org/10.3390/cells11121868.
8. Vaidyanathan, S., Trumbull, A.M., Bar, L., Rao, M., Yu, Y., and Sellers, Z.M. (2022). CFTR genotype analysis of Asians in international registries highlights disparities in the diagnosis and treatment of Asian patients with cystic fibrosis. Genet. Med. *24*, 2180–2186. https://doi.org/10.1016/j.gim.2022.06.009.
9. McGarry, M.E., and McColley, S.A. (2021). Cystic fibrosis patients of minority race and ethnicity less likely eligible for CFTR modulators based on CFTR genotype. Pediatr. Pulmonol. *56*, 1496–1503. https://doi.org/10.1002/ppul.25285.
10. Desai, M., Hine, C., Whitehouse, J.L., Brownlee, K., Charman, S.C., and Nagakumar, P. (2022). Who are the 10%? - Non eligibility of cystic fibrosis (CF) patients for highly effective modulator therapies. Respir. Med. *199*, 106878. https://doi.org/10.1016/j.rmed.2022.106878.
11. Maule, G., Ensinck, M., Bulcaen, M., and Carlon, M.S. (2021). Rewriting CFTR to cure cystic fibrosis. In Progress in Molecular Biology and Translational Science (Elsevier B.V.), pp. 185–224. https://doi.org/10.1016/bs.pmbts.2020.12.018.
12. Anzalone, A.V., Randolph, P.B., Davis, J.R., Sousa, A.A., Koblan, L.W., Levy, J.M., Chen, P.J., Wilson, C., Newby, G.A., Raguram, A., et al.

(2019). Search-and-replace genome editing without double-strand breaks or donor DNA. Nature *576*, 149–157. https://doi.org/10.1038/s41586-019-1711-4.

13. Ensinck, M.M., De Keersmaecker, L., Ramalho, A.S., Cuyx, S., Van Biervliet, S., Dupont, L., Christ, F., Debyser, Z., Vermeulen, F., and Carlon, M.S. (2022). Novel CFTR modulator combinations maximise rescue of G85E and N1303K in rectal organoids. ERJ Open Res. *8*, 00716-2021. https://doi.org/10.1183/23120541.00716-2021.
14. Bihler, H., Sivachenko, A., Millen, L., Bhatt, P., Patel, A.T., Chin, J., Bailey, V., Musisi, I., LaPan, A., Allaire, N.E., et al. (2024). In vitro modulator responsiveness of 655 CFTR variants found in people with cystic fibrosis. J. Cyst. Fibros. https://doi.org/10.1016/j.jcf.2024.02.006.
15. Yu, G., Kim, H.K., Park, J., Kwak, H., Cheong, Y., Kim, D., Kim, J., Kim, J., and Kim, H.H. (2023). Prediction of efficiencies for diverse prime editing systems in multiple cell types. Cell *186*, 2256–2272.e23. https://doi.org/10.1016/j.cell.2023.03.034.
16. Mathis, N., Allam, A., Kissling, L., Marquart, K.F., Schmidheini, L., Solari, C., Balázs, Z., Krauthammer, M., and Schwank, G. (2023). Predicting prime editing efficiency and product purity by deep learning. Nat. Biotechnol. *41*, 1151–1159. https://doi.org/10.1038/s41587-022-01613-7.
17. Kim, H.K., Yu, G., Park, J., Min, S., Lee, S., Yoon, S., and Kim, H.H. (2021). Predicting the efficiency of prime editing guide RNAs in human cells. Nat. Biotechnol. *39*, 198–206. https://doi.org/10.1038/s41587-020-0677-y.
18. Doman, J.L., Sousa, A.A., Randolph, P.B., Chen, P.J., and Liu, D.R. (2022). Designing and executing prime editing experiments in mammalian cells. Nat. Protoc. *17*, 2431–2468. https://doi.org/10.1038/s41596-022-00724-4.
19. Kluesner, M.G., Nedveck, D.A., Lahr, W.S., Garbe, J.R., Abrahante, J.E., Webber, B.R., and Moriarity, B.S. (2018). EditR: A Method to Quantify Base Editing from Sanger Sequencing. CRISPR J. *1*, 239–250. https://doi.org/10.1089/crispr.2018.0014.
20. Ensinck, M., De Keersmaecker, L., Heylen, L., Ramalho, A.S., Gijsbers, R., Farré, R., De Boeck, K., Christ, F., Debyser, Z., and Carlon, M.S. (2020). Phenotyping of Rare CFTR Mutations Reveals Distinct Trafficking and Functional Defects. Cells *9*, 754–814. https://doi.org/10.3390/cells9030754.
21. Galietta, L.V., Jayaraman, S., and Verkman, A.S. (2001). Cell-based assay for high-throughput quantitative screening of CFTR chloride transport agonists. Am. J. Physiol. Cell Physiol. *281*, C1734–C1742.
22. Veit, G., Avramescu, R.G., Chiang, A.N., Houck, S.A., Cai, Z., Peters, K.W., Hong, J.S., Pollard, H.B., Guggino, W.B., Balch, W.E., et al. (2016). From CFTR biology toward combinatorial pharmacotherapy: Expanded classification of cystic fibrosis mutations. Mol. Biol. Cell *27*, 424–433. https://doi.org/10.1091/mbc.E14-04-0935.
23. DeStefano, S., Gees, M., and Hwang, T.C. (2018). Physiological and pharmacological characterization of the N1303K mutant CFTR. J. Cyst. Fibros. *17*, 573–581. https://doi.org/10.1016/j.jcf.2018.05.011.
24. Noel, S., Sermet-Gaudelus, I., and Sheppard, D.N. (2018). N1303K: Leaving No Stone Unturned in the Search for Transformational Therapeutics (Preprint at Elsevier B.V.). https://doi.org/10.1016/j.jcf.2018.07.009.
25. Nelson, J.W., Randolph, P.B., Shen, S.P., Everette, K.A., Chen, P.J., Anzalone, A.V., An, M., Newby, G.A., Chen, J.C., Hsu, A., and Liu, D.R. (2022). Engineered pegRNAs improve prime editing efficiency. Nat. Biotechnol. *40*, 402–410. https://doi.org/10.1038/s41587-021-01039-7.
26. Chen, P.J., Hussmann, J.A., Yan, J., Knipping, F., Ravisankar, P., Chen, P.F., Chen, C., Nelson, J.W., Newby, G.A., Sahin, M., et al. (2021). Enhanced prime editing systems by manipulating cellular determinants of editing outcomes. Cell *184*, 5635–5652.e29. https://doi.org/10.1016/j.cell.2021.09.018.
27. Ferreira da Silva, J., Oliveira, G.P., Arasa-Verge, E.A., Moretton, A., Timelthaler, G., Jiricny, J., and Loizou, J.I. (2021). Prime Editing Efficiency and Fidelity are Enhanced in the Absence of Mismatch Repair. SSRN Journal, 1–17. https://doi.org/10.2139/ssrn.3921278.
28. Chen, P.J., and Liu, D.R. (2023). Prime editing for precise and highly versatile genome manipulation. Nat. Rev. Genet. *24*, 161–177. https://doi.org/10.1038/s41576-022-00541-1.
29. Ramalho, A.S., Boon, M., Proesmans, M., Vermeulen, F., Carlon, M.S., and De Boeck, K. (2022). Assays of CFTR Function In Vitro, Ex Vivo and In Vivo. Preprint at MDPI. https://doi.org/10.3390/ijms23031437.
30. Dekkers, J.F., Wiegerinck, C.L., De Jonge, H.R., Bronsveld, I., Janssens, H.M., De Winter-De Groot, K.M., Brandsma, A.M., De Jong, N.W.M., Bijvelds, M.J.C., Scholte, B.J., et al. (2013). A functional CFTR assay using primary cystic fibrosis intestinal organoids. Nat. Med. *19*, 939–945. https://doi.org/10.1038/nm.3201.
31. Vidović, D., Carlon, M.S., Da Cunha, M.F., Dekkers, J.F., Hollenhorst, M.I., Bijvelds, M.J.C., Ramalho, A.S., Van Den Haute, C., Ferrante, M., Baekelandt, V., et al. (2016). RAAV-CFTRDR rescues the cystic fibrosis phenotype in human intestinal organoids and cystic fibrosis mice. Am. J. Respir. Crit. Care Med. *193*, 288–298. https://doi.org/10.1164/rccm.201505-0914OC.
32. Alton, E.W.F.W., Beekman, J.M., Boyd, A.C., Brand, J., Carlon, M.S., Connolly, M.M., Chan, M., Conlon, S., Davidson, H.E., Davies, J.C., et al. (2017). Preparation for a first-in-man lentivirus trial in patients with cystic fibrosis. Thorax *72*, 137–147. https://doi.org/10.1136/thoraxjnl-2016-208406.
33. Maule, G., Casini, A., Montagna, C., Ramalho, A.S., De Boeck, K., Debyser, Z., Carlon, M.S., Petris, G., and Cereseto, A. (2019). Allele specific repair of splicing mutations in cystic fibrosis through AsCas12a genome editing. Nat. Commun. *10*, 3556. https://doi.org/10.1038/s41467-019-11454-9.
34. Amistadi, S., Maule, G., Ciciani, M., Ensinck, M.M., De Keersmaecker, L., Ramalho, A.S., Guidone, D., Buccirossi, M., Galietta, L.J.V., Carlon, M.S., and Cereseto, A. (2023). Functional restoration of a CFTR splicing mutation through RNA delivery of CRISPR adenine base. Mol. Ther. *31*, 1647–1660. https://doi.org/10.1016/j.ymthe.2023.03.004.
35. Berkers, G., van Mourik, P., Vonk, A.M., Kruisselbrink, E., Dekkers, J.F., de Winter-de Groot, K.M., Arets, H.G.M., Marck-van der Wilt, R.E.P., Dijkema, J.S., Vanderschuren, M.M., et al. (2019). Rectal Organoids Enable Personalized Treatment of Cystic Fibrosis. Cell Rep. *26*, 1701–1708.e3. https://doi.org/10.1016/j.celrep.2019.01.068.
36. Muilwijk, D., de Poel, E., van Mourik, P., Suen, S.W.F., Vonk, A.M., Brunsveld, J.E., Kruisselbrink, E., Oppelaar, H., Hagemeijer, M.C., Berkers, G., et al. (2022). Forskolin-induced organoid swelling is associated with long-term cystic fibrosis disease progression. Eur. Respir. J. *60*, 2100508. https://doi.org/10.1183/13993003.00508-2021.
37. Dekkers, J.F., Berkers, G., Kruisselbrink, E., Vonk, A., De Jonge, H.R., Janssens, H.M., Bronsveld, I., Van De Graaf, E.A., Nieuwenhuis, E.E.S., Houwen, R.H.J., et al. (2016). Characterizing responses to CFTR-modulating drugs using rectal organoids derived from subjects with cystic fibrosis. Sci. Transl. Med. *8*, 344ra84. https://doi.org/10.1126/scitranslmed.aad8278.
38. Valley, H.C., Bukis, K.M., Bell, A., Cheng, Y., Wong, E., Jordan, N.J., Allaire, N.E., Sivachenko, A., Liang, F., Bihler, H., et al. (2019). Isogenic cell models of cystic fibrosis-causing variants in natively expressing pulmonary epithelial cells. J. Cyst. Fibros. *18*, 476–483. https://doi.org/10.1016/j.jcf.2018.12.001.
39. Cozens, A.L., Yezzi, M.J., Kunzelmann, K., Ohrui, T., Chin, L., Eng, K., Finkbeiner, W.E., Widdicombe, J.H., and Gruenert, D.C. (1994). CFTR expression and chloride secretion in polarized immortal human bronchial epithelial cells. Am. J. Respir. Cell Mol. Biol. *10*, 38–47.
40. Concordet, J.P., and Haeussler, M. (2018). CRISPOR: Intuitive guide selection for CRISPR/Cas9 genome editing experiments and screens. Nucleic Acids Res. *46*, W242–W245. https://doi.org/10.1093/nar/gky354.
41. Doench, J.G., Fusi, N., Sullender, M., Hegde, M., Vaimberg, E.W., Donovan, K.F., Smith, I., Tothova, Z., Wilen, C., Orchard, R., et al. (2016). Optimized sgRNA design to maximize activity and minimize off-target effects

of CRISPR-Cas9. Nat. Biotechnol. *34*, 184–191. https://doi.org/10.1038/nbt.3437.

42. Tsai, S.Q., Zheng, Z., Nguyen, N.T., Liebers, M., Topkar, V.V., Thapar, V., Wyvekens, N., Khayter, C., Iafrate, A.J., Le, L.P., et al. (2015). GUIDE-seq enables genome-wide profiling of off-target cleavage by CRISPR-Cas nucleases. Nat. Biotechnol. *33*, 187–197. https://doi.org/10.1038/nbt.3117.
43. Schwank, G., Koo, B.K., Sasselli, V., Dekkers, J.F., Heo, I., Demircan, T., Sasaki, N., Boymans, S., Cuppen, E., Van Der Ent, C.K., et al. (2013). Functional repair of CFTR by CRISPR/Cas9 in intestinal stem cell organoids of cystic fibrosis patients. Cell Stem Cell *13*, 653–658. https://doi.org/10.1016/j.stem.2013.11.002.
44. Hollywood, J.A., Lee, C.M., Scallan, M.F., and Harrison, P.T. (2016). Analysis of gene repair tracts from Cas9/gRNA double-stranded breaks in the human CFTR gene. Sci. Rep. *6*, 32230–32312. https://doi.org/10.1038/srep32230.
45. Vaidyanathan, S., Baik, R., Chen, L., Bravo, D.T., Suarez, C.J., Abazari, S.M., Salahudeen, A.A., Dudek, A.M., Teran, C.A., Davis, T.H., et al. (2022). Targeted replacement of full-length CFTR in human airway stem cells by CRISPR-Cas9 for pan-mutation correction in the endogenous locus. Mol. Ther. *30*, 223–237. https://doi.org/10.1016/j.ymthe.2021.03.023.
46. Vaidyanathan, S., Salahudeen, A.A., Sellers, Z.M., Bravo, D.T., Choi, S.S., Batish, A., Le, W., Baik, R., de la O, S., Kaushik, M.P., et al. (2020). High-Efficiency, Selection-free Gene Repair in Airway Stem Cells from Cystic Fibrosis Patients Rescues CFTR Function in Differentiated Epithelia. Cell Stem Cell *26*, 161–171.e4. https://doi.org/10.1016/j.stem.2019.11.002.
47. Leibowitz, M.L., Papathanasiou, S., Doerfler, P.A., Blaine, L.J., Sun, L., Yao, Y., Zhang, C.Z., Weiss, M.J., and Pellman, D. (2021). Chromothripsis as an on-target consequence of CRISPR–Cas9 genome editing. Nat. Genet. *53*, 895–905. https://doi.org/10.1038/s41588-021-00838-7.
48. Zuccaro, M.V., Xu, J., Mitchell, C., Marin, D., Zimmerman, R., Rana, B., Weinstein, E., King, R.T., Palmerola, K.L., Smith, M.E., et al. (2020). Allele-Specific Chromosome Removal after Cas9 Cleavage in Human Embryos. Cell *183*, 1650–1664.e15. https://doi.org/10.1016/j.cell.2020.10.025.
49. Haapaniemi, E., Botla, S., Persson, J., Schmierer, B., and Taipale, J. (2018). CRISPR-Cas9 genome editing induces a p53-mediated DNA damage response. Nat. Med. *24*, 927–930. https://doi.org/10.1038/s41591-018-0049-z.
50. Kosicki, M., Tomberg, K., and Bradley, A. (2018). Repair of double-strand breaks induced by CRISPR–Cas9 leads to large deletions and complex rearrangements. Nat. Biotechnol. *36*, 765–771. https://doi.org/10.1038/nbt.4192.
51. Bulcaen, M., and Carlon, M.S. (2024). Genetic surgery for a cystic fibrosis-causing splicing mutation. Mol. Ther. Methods Clin. Dev. *32*, 101177.
52. Li, X., Chen, W., Martin, B.K., Calderon, D., Lee, C., Choi, J., Chardon, F.M., Mcdiarmid, T., Kim, H., Lalanne, J.-B., et al. (2024). Chromatin context-dependent regulation and epigenetic manipulation of prime editing. Cell. https://doi.org/10.1016/j.cell.2024.03.020.
53. Geurts, M.H., de Poel, E., Pleguezuelos-Manzano, C., Oka, R., Carrillo, L., Andersson-Rolf, A., Boretto, M., Brunsveld, J.E., van Boxtel, R., Beekman, J.M., and Clevers, H. (2021). Evaluating CRISPR-based prime editing for cancer modeling and CFTR repair in organoids. Life Sci. Alliance *4*, 2020009400–e202001012. https://doi.org/10.26508/LSA.202000940.
54. Schene, I.F., Joore, I.P., Baijens, J.H.L., Stevelink, R., Kok, G., Shehata, S., Ilcken, E.F., Nieuwenhuis, E.C.M., Bolhuis, D.P., van Rees, R.C.M., et al. (2022). Mutation-specific reporter for optimization and enrichment of prime editing. Nat. Commun. *13*, 1028–1110. https://doi.org/10.1038/s41467-022-28656-3.
55. Pranke, I.M., Hatton, A., Simonin, J., Jais, J.P., Le Pimpec-Barthes, F., Carsin, A., Bonnette, P., Fayon, M., Stremler-Le Bel, N., Grenet, D., et al. (2017). Correction of CFTR function in nasal epithelial cells from cystic fibrosis patients predicts improvement of respiratory function by CFTR modulators. Sci. Rep. *7*, 7375. https://doi.org/10.1038/s41598-017-07504-1.
56. Pranke, I., Hatton, A., Masson, A., Flament, T., Le Bourgeois, M., Chedevergne, F., Bailly, C., Urbach, V., Hinzpeter, A., Edelman, A., et al. (2019). Might Brushed Nasal Cells Be a Surrogate for CFTR Modulator Clinical Response? (Preprint at American Thoracic Society). https://doi.org/10.1164/rccm.201808-1436LE.
57. Sermet-Gaudelus, I., Girodon, E., Vermeulen, F., Solomon, G.M., Melotti, P., Graeber, S.Y., Bronsveld, I., Rowe, S.M., Wilschanski, M., Tümmler, B., et al. (2022). ECFS standards of care on CFTR-related disorders: Diagnostic criteria of CFTR dysfunction. J. Cyst. Fibros. *21*, 922–936. https://doi.org/10.1016/j.jcf.2022.09.005.
58. Dreano, E., Régis Burgel, P., Hatton, A., Bouazza, N., Chevalier, B., Macey, J., Leroy, S., Durieu, I., Weiss, L., Grenet, D., et al. (2023). Theratyping Cystic Fibrosis patients to guide Elexacaftor-Tezacaftor-Ivacaftor out of label prescription. Eur. Respir. J. *62*, 2300110.
59. Borten, M.A., Bajikar, S.S., Sasaki, N., Clevers, H., and Janes, K.A. (2018). Automated brightfield morphometry of 3D organoid populations by OrganoSeg. Sci. Rep. *8*, 5319. https://doi.org/10.1038/s41598-017-18815-8.
60. Gritti, N., Le Lim, J., Anlaş, K., Pandya, M., Aalderink, G., Martınez-Ara, G., and Trivedi, V. (2021). Morgana: Accessible quantitative analysis of Organoids with machine learning. Development *148*, dev199611. https://doi.org/10.1242/DEV.199611.
61. Kassis, T., Hernandez-Gordillo, V., Langer, R., and Griffith, L.G. (2019). OrgaQuant: Human Intestinal Organoid Localization and Quantification Using Deep Convolutional Neural Networks. Sci. Rep. *9*, 12479. https://doi.org/10.1038/s41598-019-48874-y.
62. Cuyx, S., Ramalho, A.S., Corthout, N., Fieuws, S., Fürstová, E., Arnauts, K., Ferrante, M., Verfaillie, C., Munck, S., Boon, M., et al. (2021). Rectal organoid morphology analysis (ROMA) as a promising diagnostic tool in cystic fibrosis. Thorax *76*, 1146–1149. https://doi.org/10.1136/thoraxjnl-2020-216368.
63. Schene, I.F., Joore, I.P., Oka, R., Mokry, M., van Vugt, A.H.M., van Boxtel, R., van der Doef, H.P.J., van der Laan, L.J.W., Verstegen, M.M.A., van Hasselt, P.M., et al. (2020). Prime editing for functional repair in patient-derived disease models. Nat. Commun. *11*, 5352–5358. https://doi.org/10.1038/s41467-020-19136-7.
64. Liang, S.Q., Liu, P., Ponnienselvan, K., Suresh, S., Chen, Z., Kramme, C., Chatterjee, P., Zhu, L.J., Sontheimer, E.J., Xue, W., and Wolfe, S.A. (2023). Genome-wide profiling of prime editor off-target sites in vitro and in vivo using PE-tag. Nat. Methods *20*, 898–907. https://doi.org/10.1038/s41592-023-01859-2.
65. Gao, R., Fu, Z.C., Li, X., Wang, Y., Wei, J., Li, G., Wang, L., Wu, J., Huang, X., Yang, L., and Chen, J. (2022). Genomic and Transcriptomic Analyses of Prime Editing Guide RNA-Independent Off-Target Effects by Prime Editors. CRISPR J. *5*, 276–293. https://doi.org/10.1089/crispr.2021.0080.
66. Vakulskas, C.A., and Behlke, M.A. (2019). Evaluation and reduction of crispr off-target cleavage events. Nucleic Acid Ther. *29*, 167–174. https://doi.org/10.1089/nat.2019.0790.
67. Frangoul, H., Altshuler, D., Cappellini, M.D., Chen, Y.-S., Domm, J., Eustace, B.K., Foell, J., de la Fuente, J., Grupp, S., Handgretinger, R., et al. (2021). CRISPR-Cas9 Gene Editing for Sickle Cell Disease and β-Thalassemia. N. Engl. J. Med. *384*, 252–260. https://doi.org/10.1056/nejmoa2031054.
68. Nguengang Wakap, S., Lambert, D.M., Olry, A., Rodwell, C., Gueydan, C., Lanneau, V., Murphy, D., Le Cam, Y., and Rath, A. (2020). Estimating cumulative point prevalence of rare diseases: analysis of the Orphanet database. Eur. J. Hum. Genet. *28*, 165–173. https://doi.org/10.1038/s41431-019-0508-0.
69. Mayer-Hamblett, N., van Koningsbruggen-Rietschel, S., Nichols, D.P., VanDevanter, D.R., Davies, J.C., Lee, T., Durmowicz, A.G., Ratjen, F., Konstan, M.W., Pearson, K., et al. (2020). Building Global Development Strategies for CF Therapeutics during a Transitional CFTR Modulator Era (Preprint at Elsevier B.V.). https://doi.org/10.1016/j.jcf.2020.05.011.

70. Urnov, F.D. (2021). Imagine CRISPR cures. Mol. Ther. *29*, 3103–3106. https://doi.org/10.1016/j.ymthe.2021.10.019.

71. Yarnall, M.T.N., Ioannidi, E.I., Schmitt-Ulms, C., Krajeski, R.N., Lim, J., Villiger, L., Zhou, W., Jiang, K., Garushyants, S.K., Roberts, N., et al. (2023). Drag-and-drop genome insertion of large sequences without double-strand DNA cleavage using CRISPR-directed integrases. Nat. Biotechnol. *41*, 500–512. https://doi.org/10.1038/s41587-022-01527-4.

72. Anzalone, A.V., Gao, X.D., Podracky, C.J., Nelson, A.T., Koblan, L.W., Raguram, A., Levy, J.M., Mercer, J.A.M., and Liu, D.R. (2022). Programmable deletion, replacement, integration and inversion of large DNA sequences with twin prime editing. Nat. Biotechnol. *40*, 731–740. https://doi.org/10.1038/s41587-021-01133-w.

73. U.S. Food & Drug Administration (2017). FDA expands approved use of Kalydeco to treat additional mutations of cystic fibrosis. https://www.fda.gov/news-events/press-announcements/fda-expands-approved-use-kalydeco-treat-additional-mutations-cystic-fibrosis.

74. Vertex Pharmaceuticals (2020). Vertex announces FDA approvals of Trikafta®(Elexacaftor/Tezacaftor/Ivacaftor and SYMDEKO®(Tezacaftor/Ivacaftor) and KALYDECO®(Ivacaftor) for use in people with CF with certain rare mutations. https://investors.vrtx.com/news-releases/news-release-details/vertex-announces-fda-approvals-trikaftar.

75. Ramalho, A.S., Förstová, E., Vonk, A.M., Ferrante, M., Verfaillie, C., Dupont, L., Boon, M., Proesmans, M., Beekma, J.M., Sarouk, I., et al. (2021). Correction of CFTR function in intestinal organoids to guide treatment of cystic fibrosis. Eur. Respir. J. *57*. https://doi.org/10.1183/13993003.02426-2019.

76. Zierden, H.C., Josyula, A., Shapiro, R.L., Hsueh, H.T., Hanes, J., and Ensign, L.M. (2021). Avoiding a Sticky Situation: Bypassing the Mucus Barrier for Improved Local Drug Delivery. Trends Mol. Med. *27*, 436–450. https://doi.org/10.1016/j.molmed.2020.12.001.

77. Sato, Y., Mustafina, K.R., Luo, Y., Martini, C., Thomas, D.Y., Wiseman, P.W., and Hanrahan, J.W. (2021). Nonspecific binding of common anti-CFTR antibodies in ciliated cells of human airway epithelium. Sci. Rep. *11*, 23256. https://doi.org/10.1038/s41598-021-02420-x.

78. Galietta, L.J., Haggie, P.M., and Verkman, A.S. (2001). Green fluorescent protein-based halide indicators with improved chloride and iodide affinities. FEBS Lett. *499*, 220–224. https://doi.org/10.1016/S0014-5793(01)02561-3.

79. Clement, K., Rees, H., Canver, M.C., Gehrke, J.M., Farouni, R., Hsu, J.Y., Cole, M.A., Liu, D.R., Joung, J.K., Bauer, D.E., and Pinello, L. (2019). CRISPResso2 provides accurate and rapid genome editing sequence analysis. Nat. Biotechnol. *37*, 224–226. https://doi.org/10.1038/s41587-019-0032-3.

80. Vonk, A.M., van Mourik, P., Ramalho, A.S., Silva, I.A.L., Statia, M., Kruisselbrink, E., Suen, S.W.F., Dekkers, J.F., Vleggaar, F.P., Houwen, R.H.J., et al. (2020). Protocol for Application, Standardization and Validation of the Forskolin-Induced Swelling Assay in Cystic Fibrosis Human Colon Organoids. STAR Protoc. *1*, 100019. https://doi.org/10.1016/j.xpro.2020.100019.

81. Ibrahimi, A., Velde, G.V., Reumers, V., Toelen, J., Thiry, I., Vandeputte, C., Vets, S., Deroose, C., Bormans, G., Baekelandt, V., et al. (2009). Highly Efficient Multicistronic Lentiviral Vectors with Peptide 2A Sequences. Hum. Gene Ther. *20*, 845–860.

82. Sharma, M., Pampinella, F., Nemes, C., Benharouga, M., So, J., Du, K., Bache, K.G., Papsin, B., Zerangue, N., Stenmark, H., and Lukacs, G.L. (2004). Misfolding diverts CFTR from recycling to degradation: Quality control at early endosomes. J. Cell Biol. *164*, 923–933. https://doi.org/10.1083/jcb.200312018.

83. Cheng, Z.-Q., Dai, Q., Li, H., Song, J., Wu, X., and Hauptmann, A.G. (2022). Rethinking Spatial Invariance of Convolutional Networks for Object Counting. arXiv. https://doi.org/10.1109/CVPR52688.2022.01902.

84. Song, Q., Wang, C., Jiang, Z., Wang, Y., Tai, Y., Wang, C., Li, J., Huang, F., and Wu, Y. (2021). Rethinking counting and localization in crowds: a purely point-based framework. arXiv. https://doi.org/10.48550/arXiv.2206.05253.

85. Idrees, H., Tayyab, M., Athrey, K., Zhang, D., Al-Maadeed, S., Rajpoot, N., and Shah, M. (2018). Composition loss for counting, density map estimation and localization in dense crowds. arXiv. https://doi.org/10.48550/arXiv.1808.01050.

86. Russell, B.C., Torralba, A., Murphy, K.P., and Freeman, W.T. (2008). LabelMe: A database and web-based tool for image annotation. Int. J. Comput. Vis. *77*, 157–173. https://doi.org/10.1007/s11263-007-0090-8.

87. Simonyan, K., and Zisserman, A. (2014). Very deep convolutional networks for large-scale image recognition. arXiv. https://doi.org/10.48550/arXiv.1409.1556.

88. Ma, Z., Wei, X., Hong, X., Gong, Y., et al. (2022). Bayesian loss for crowd count estimation with point supervision. arXiv. https://doi.org/10.48550/arXiv.2207.02696.

89. Wang, C.-Y., Bochkovskiy, A., Liao, H.-Y.M., Gong, Y., et al. (2022). YOLOv7: Trainable bag-of-freebies sets new state-of-the-art for real-time object detectors. arXiv. https://doi.org/10.48550/arXiv.2207.02696.

90. Pedrazzoli, E., Bianchi, A., Umbach, A., Amistadi, S., Brusson, M., Frati, G., Ciciani, M., Badowska, K.A., Arosio, D., Miccio, A., et al. (2023). An optimized SpCas9 high-fidelity variant for direct protein delivery. Mol. Ther. *31*, 2257–2265. https://doi.org/10.1016/j.ymthe.2023.03.007.

91. Nobles, C.L., Reddy, S., Salas-Mckee, J., Liu, X., June, C.H., Melenhorst, J.J., Davis, M.M., Zhao, Y., and Bushman, F.D. (2019). IGUIDE: An improved pipeline for analyzing CRISPR cleavage specificity. Genome Biol. *20*, 14. https://doi.org/10.1186/s13059-019-1625-3.

STAR★METHODS

KEY RESOURCES TABLE

REAGENT or RESOURCE	SOURCE	IDENTIFIER
Antibodies		
Calnexin polyclonal Ab	Thermo Fisher Scientific	PA5-34754; RRID: AB_2552106
CFF CFTR-Ab570	Cystic Fibrosis Foundation	Ab570
CFF CFTR-Ab596	Cystic Fibrosis Foundation	Ab596
CFF CFTR-Ab660	Cystic Fibrosis Foundation	Ab660
Goat anti-mouse Alexa 488	Thermo Fisher Scientific	A-28175; RRID: AB_2536161
Goat anti-mouse HRP	Agilent	P044701-2; RRID: AB_2617137
Goat anti-rabbit Alexa 633	Thermo Fisher Scientific	A-21070; RRID: AB_2535731
HA11	Biolegend	901515; RRID: AB_2565336
Mouse anti-beta-tubulin	Sigma Aldrich	T7941; RRID: AB_261775
Mouse anti MUC5AC	Abcam	Ab3649; RRID: AB_2146844
Mouse anti-cytokeratin 5	Leica Biosystems	NCL-L-CK5; RRID: AB_563807
Biological samples		
Rectal organoids derived from people with Cystic Fibrosis	KU/UZ Leuven	N/A
Human nasal epithelium (HNE) cells	Institut Necker Enfants Malades, KU Leuven	N/A
Chemicals, peptides, and recombinant proteins		
Lipofectamine 3000	Thermo Fisher Scientific	L3000008
NuPage Tris-Acetate polyacrylamide gel	Thermo Fisher Scientific	WG1602A
Y-27632	Selleckchem	S0149
Collagen IV	Merck	C7521
Pneumacult™ Ex Plus	StemCell Technologies	05040
Pneumacult™ ALI	StemCell Technologies	05001
Forskolin	Sigma	F3917
Critical commercial assays		
iProof polymerase kit	BioRad	1725302
GeneArt Gibson assembly kit	Thermo Fisher Scientific	A46627
P24 INNOTEST® HIV ELISA	Fujirebio	80563
BCA protein assay kit	Thermo Fisher Scientific	23225
Trans-Blot Turbo Transfer System	BioRad	1704150
Illumina Reagent kit V2-150PE	Illumina	V2-150PE
NovaSeq 6000 S4 Reagent Kit v1.5	Illumina	20028312
Deposited data		
GUIDE-seq raw sequencing reads	This paper	https://dataview.ncbi.nlm.nih.gov/object/PRJNA997578
Targeted deep sequencing	This paper	https://dataview.ncbi.nlm.nih.gov/object/PRJNA997578
Experimental models: Cell lines		
HEK293T cell lines with single integrated copy of WT/mutant *CFTR* cDNA with extracellular 3HA-tag	This paper. Ensinck et al.[20]	HEK293T-L227R-3HA-CFTR, HEK293T-N1303K-3HA-CFTR, HEK293T-3HA-WT-CFTR
Parental 16HBE cells	Milipore	16HBE
16HBEge	Cystic Fibrosis Foundation Valley et al.[12]	16HBEgeN1303K-CFTR
HS-YFP engineered 16HBE cell lines	This paper	NA

(*Continued on next page*)

Continued

REAGENT or RESOURCE	SOURCE	IDENTIFIER
Oligonucleotides		
pegRNA and ngRNA designs	This paper	See Table S1
Single-stranded DNA oligos for cloning	IDT	see Table S2
Custom double stranded DNA (gBlock)	IDT	see Table S2
Primers for NGS	IDT	see Table S3
Recombinant DNA		
pCMV-PE2 plasmid	Anzalone et al.[12]	Addgene: 132777
pCMV-PEmax-P2A-MLH1dn plasmid	Chen et al.[26]	Addgene: 174828
pU6-pegRNA-GG-acceptor plasmid	Anzalone et al.[12]	Addgene: 132775
pU6-tevopreQ1-GG-acceptor plasmid	Nelson et al.[25]	Addgene: 174038
lentiCRISPRv2 plasmid	Sanjana et al.	Addgene: 52961
Lenti-CMV-PE2-IRES-ZeoR plasmid	This paper	Addgene: 207352
HS-eYFP (F46L-H148Q-I152L) plasmid	Galietta et al.[78]	N/A
Lenti-CMV-PEmax-IRES-ZeoR plasmid	This paper	Addgene: 207353
Lenti-CMV-MLH1dn-IRES-puroR	This paper	Addgene: 207354
Lenti-RNF2-tevopreq1-epegRNA+5G>T_EF1a-puroR	This paper	Addgene: 207355
Lenti-N1303K-tevopreq1-epegRNA+13C>G_EF1a-puro (PBS 14- RTT 18)	This paper	Addgene: 207356
Lenti-L227R-tevopreq1-epegRNA+13C>A_EF1a-puroR (PBS 10 – RTT 19)	This paper	Addgene: 207357
Lenti-RNF2-ngRNA+41_EF1a-puroR	This paper	Addgene: 207358
Lenti-N1303K-ngRNA+14_EF1a-puroR	This paper	Addgene: 207359
Lenti-L227R-ngRNA+15_EF1a-puroR	This paper	Addgene: 207360
Software and algorithms		
EditR	Kluesner et al.[19]	http://baseeditr.com
DETECTOR organoid analysis tool	This paper	https://github.com/RL-arch/detector
CRISPOR	Concordet et al.[40,42]	http://crispor.tefor.net
GUIDE-seq	Tsai et al.[42]	https://github.com/aryeelab/guideseq
Crispresso2	Clement et al.[79]	http://crispresso2.pinellolab.org/submission
Other		
Lentiviral vectors	Leuven Viral Vector Core (LVVC)	Custom orders
ImageQuant 800 Fluor western blot imager	GE Healthcare	Amersham ImageQuant 800 Fluor
Envision multimode plate reader	Perkin Elmer	2105-0010
Ussing set-up for HNE electrophysiology	World Precision instruments	EVC4000 V/I clamp

RESOURCE AVAILABILITY

Lead contact

Further information and requests for resources and reagents should be directed to and will be fulfilled by the lead contact, Dr. Marianne Carlon (marianne.carlon@kuleuven.be).

Materials availability

All materials generated during this study are available upon reasonable request and material transfer agreement.

Following plasmids have been deposited to Addgene: lenti-pU6-tevopreq1-L227R-epegRNA+13C>A_EF1a-puro (Addgene: 207357), lenti-pU6-L227R-ngRNA+15_EF1a-puro (Addgene: 207360), lenti-pU6-tevopreq1-N1303K-epegRNA+13C>G_EF1a-puro (Addgene: 207356), lenti-pU6-N1303K-ngRNA+14_EF1a-puro (Addgene: 207359), lenti-pU6-tevopreq1-RNF2-epegRNA+5G>T_EF1a-puro (Addgene: 207355), lenti-pU6-RNF2-ngRNA+41_EF1a-puro (Addgene: 207358), lenti-pCMV-MLH1dn-ires-zeoR (Addgene: 207354), lenti-pCMV-PE2-ires-zeo (Addgene: 207352), lenti-pCMV-PEmax (Addgene: 207353).

Data and code availability

- GUIDE-Seq and targeted deep sequencing data has been deposited at NCBI-Sequence Read Archive (SRA) and are publicly available as of the date of publication. Accession numbers are listed in the key resources table. Original western blot images are available as supplementary data.
- All original code has been deposited at Dataverse and is publicly available as of the date of publication. DOIs are listed in the key resources table.
- Any additional information required to reanalyse the data reported in this paper is available from the lead contact upon request.
- The DETE*C*TOR tool for automated organoid analysis is freely accessible from Dataverse (https://doi.org/10.7910/DVN/OZZRPG) and Github https://github.com/RL-arch/detector.

EXPERIMENTAL MODEL AND STUDY PARTICIPANT DETAILS

Cell lines

In this work HEK293T and 16HBE cells were engineered and used for readout of *CFTR* correction and associated rescue in CFTR ion channel function. HEK293T cells were purchased at ATCC (CRL-3216) and originate from a female individual. The engineered HEK293T 3HA-N1303K-CFTR and HEK293T 3HA-WT-CFTR models were described previously.[20] The HEK293T 3HA-L227R-CFTR cell model was generated as part of this study by transducing parental HEK293T cell lines with a lentiviral vector encoding the 3HA-L227R-CFTR cDNA at low MOI and selection for a single integrated copy.

Parental 16HBE14o-cell lines were originally derived from a male individual, described here[39] and were obtained from Millipore ((#SCC150). The Cystic Fibrosis Foundation performed gene editing at the *CFTR* locus on both alleles of the parental 16HBE14o to obtain isogenic variants (16HBEge) of specific CFTR variants, including N1303K, facilitating CF research[38] (https://www.cff.org/researchers/cell-model-resources).

In our studies, we modified these 16HBEge cell lines by stably introducing an HS-YFP sensor to enable functional evaluation of *CFTR* gene correction. For this purpose, parental 16HBE and 16HBEgeN1303K were transduced with lentiviral vectors encoding the HS-YFP sensor in tandem with a zeocin selection cassette. Following transduction at low MOI, cells were selected for integration of the sensor and used for functional assays. To investigate the effect of MLH1dn on prime editing in 16HBE cells, a double-positive 16HBE cell line was generated following the same procedure using puromycin selection (16HBEgeN1303K_HS-YFP_MLH1dn). Culture conditions are described in the STAR Methods section.

All the derivatives generated from the different parental cell lines are biobanked at KU Leuven with approval by the UZ Leuven ethical committee and biobank services (S67110, S67338) and are available upon request.

Primary cell cultures

Human rectal organoids were generated from rectal biopsies of PwCF as previously described[80] and biobanked following successful culture. Informed consent was obtained prior to biopsy collection, in accordance with the ethical committee of UZ Leuven (S56329, S67338). Specifically, biobanked samples from PwCF homozygous or heterozygous for L227R (L227R/L227R, L227R/F508del) or N1303K (N1303K/N1303K, N1303K/F508del, N1303K/3121-1A>G; $n = 1$ for each) were used for this study.

Human nasal epithelium (HNE) cells from pwCF harboring L227R or N1303K alleles (L227R/L227R, N1303K/N1303K and N1303K/R1162X, $n = 1$ each) were collected and biobanked as previously described.[55] Written informed consent was obtained from each adult PwCF or parent for those aged 12 to 18 years (AFSSAPS (ANSM) B1005423–40, n° Eudract 2010-A00392-37; CPP IDF2: 2010-05-03-3).

Culture and biobanking conditions are described in the STAR Methods section.

METHOD DETAILS

Plasmids

All restriction enzymes used for cloning were ordered from Thermo Fisher Scientific (MA, USA), all primers and custom nucleic acid sequences were ordered from IDT (Belgium). The pCHMWS-3HA-L227R-CFTR-IRES-puro lentiviral (LV) transfer construct was generated via insertion of a L227R-*CFTR* exon1-8 gBlock sequence ordered from IDT (Table S1) and inserted via XbaI and BsrGI (ER0681 and ER0931) digestion into the pCHMWS-EC3HA-WT-CFTR described previously[20] using T4 ligase (EL0016, Thermo Fisher Scientific, MA, USA). The pCMV-PE2 (Addgene: 32775), pCMV-PEmax-P2A-MLH1dn (Addgene: 174828), pU6-pegRNA-GG-acceptor (Addgene: 132777) and pU6-tevopreQ1-GG-acceptor (Addgene: 174038) plasmids were kind gifts of David Liu. (e)pegRNA spacer, scaffold and 3′ extension sequences were ordered as single stranded oligodeoxynucleotides (ssODNs) (Table S2), annealed and ligated into pegRNA and epegRNA acceptor plasmids via Golden Gate assembly as described in Anzalone et al.[12] and Nelson et al.[25] For pU6-ngRNA constructs, spacer sequences were ordered as compatible ssODNs (Table S2), annealed and ligated using T4 ligase into a BpiI (ER1011)-restricted backbone containing hU6 promoter and *Sp*Cas9 single guide (sgRNA) scaffold. For the generation of the pCHMWS-PE2-ires-zeo lenti-transfer construct, PE2 was amplified using iProof polymerase (#1725302, BioRad, CA, USA) from pCMV-PE2 via PCR primers with XbaI and BsrGI sites attached to the 5′ ends (Table S2). The amplified insert was ligated into an LV backbone using XbaI and BsrGI. Cloning of a similar LV-PEmax construct was ordered from Genscript (NJ, USA). To obtain

a pU6-ngRNA landing construct compatible with lentiviral vector production, the SpCas9 coding sequence from lentiCRISPRv2 (gift from Feng Zhang, Addgene: 52961) was removed via digestion with XbaI and BamHI (ER0681 and ER0051) followed by T4 ligase-mediated ligation of a custom adaptor (Table S2). This construct was subsequently used to clone LV-pU6-ngRNA_EF1a-puro constructs via Esp3I (ER0451) digestion and T4 ligase ligation. To generate an LV-pU6-pegRNA_EF1a-puro LV-transfer constructs, the pU6-ngRNA cassette of LV-pU6-RNF2-ngRNA_EF1a-puro was interchanged with the pU6-pegRNA cassette from pU6-pegRNA-GG-acceptor via iProof PCR-amplification using primers containing NheI (ER0971) restriction sites (Table S2). Once generated this construct allows straightforward insertion of any pegRNA/epegRNA cloned in the backbones from the Liu lab using KpnI (ER0521). The pCHMWS-HS-YFP-ires-zeo construct was cloned via insertion of a custom HS-YFP-ires-zeo gene Block (Table S2) in the pCHMWS-3HA-CFTR-ires-puro backbone via MluI/XbaI digestion (ER0561/ER068). MLH1dn was amplified from pCMV-PEmax-P2A-MLH1dn and cloned into pCHMWS-YFP-ires-zeo backbone using custom primers (Table S2) and Gibson assembly (GeneArt kit, A46627, Fisher Thermo Scientific, MA, USA).

Viral vector production

Serum-free viral vectors were ordered from Leuven Viral Vector Core and produced as previously described.[81] In short, HEK293T cells were seeded in five 10 cm diameter petri dishes (353003, BD Biosciences, CA, USA) and triple transfected with the LV transfer plasmids described above, the packaging plasmid (pCMVΔR8.91) and a VSV-G envelope plasmid using linear polyethylenimine (23966-1, PEI, Polysciences Europe, Germany). Supernatant containing lentiviral particles was harvested 48h and 72h post transfection and filtered through a 0.45μm pore-size filter (SLHA033SS, Merck Milipore, MA, USA). The viral vector titer was determined via p24 INNOTEST HIV ELISA (80563, Fujirebio, Belgium). The resulting lentiviral vectors are referred to as LV.

Cell lines and transfection

HEK293T NT cells and HEK293T cells stably expressing 3HA-WT-CFTR, 3HA-L227R and 3HA-N1303K-CFTR were cultured in Dulbecco's modified Eagle's medium (DMEM, 61965026, Gibco, MA, USA) supplemented with 8% FBS and 50μg/mL gentamicin (15750045, Thermo Fisher Scientific, MA, USA). WT or mutant expressing HEK293T cell lines were kept on 2 μg/mL puromycin and passaged every 2/3 days using Trypsin-EDTA 0.25% phenol red (25200056, Gibco, MA, USA). For transfection, 250.000 cells were seeded in 24 well plates (734–2325, VWR, PA, USA) in 1 mL DMEM +8%FBS + gentamicin medium. 24 h after cell seeding, transfection mixes were made by complexing 750 ng PE plasmid +250 ng (e)pegRNA plasmid +83 ng ngRNA plasmid with 3 μL Lipofectamine 3000 and 1 μL P3000 Reagent (L3000008, Thermo Fisher Scientific, MA, USA). Both the plasmids and transfection reagents were dissolved in 50 μL Opti-MEM, subsequently pipetted together and allowed to form complexes for 10 min at room temperature. Afterward, 0.5 mL culture medium was removed, and transfection mixes were carefully added. For HS-YFP assays following plasmid ratios were used: 100 ng HS-YFP (F46L-H148Q-I152L) + 675 ng PE + 225 ng (e)pegRNA +75 ng ngRNA. Transfected cells were split to 6 well plates (734–0991, VWR, PA, USA) 24 h post transfection and harvested 72h after transfection using 0.25% Trypsin/EDTA.

16HBE cells were cultured using MEM (11095-072, Gibco, MA, USA) supplemented with 10% FBS and gentamicin (50 μg/mL). Culture flasks were coated with following solution for >2h at 37°C: 48 mL LHC-8 basal medium (12677-027, Gibco, CA, USA), 67 μL Bovine serum albumin fraction V 7.5% (15260-037, Gibco, CA, USA), 500 μL PureCol (3 mg/mL, 5005-100mL, Advanced BioMatrix, CA, USA), 500 μL fibronectin from human plasma (1 mg/mL, 33016-015, Thermo Fisher Scientific, MA, USA). Medium was replaced every 2/3 days and cells were passaged once a week.

Generation of HEK293T and 16HBE cell lines

HEK293T cells stably expressing 3HA-N1303K-CFTR and 3HA-WT-CFTR have been previously generated and characterized.[13,20,82] The 3HA-L227R HEK293T cell line was generated via LV transduction with vectors generated from the pCHMWS-3HA-L227R-CFTR-ires-puro. HEK293T cells were transduced with a 1/3 serial vector dilution and selected using puromycin (2 μg/mL, ant-pr-1, Invivogen, CA, USA) to obtain a single integrated copy stable cell line.

HS-YFP-expressing 16HBE cell lines were generated via transduction with 1/3 dilution series of LV-CMV-HS-YFP-IRES-ZeoR vector followed by selection for a single integrated copy with zeocin (100 μg/mL, ant-zn-5b, Invivogen, CA, USA).

DNA extraction and sanger sequencing

For readout of prime editing at the DNA level, Sanger sequencing and EditR software[19] were used, unless mentioned otherwise. Genomic DNA extraction was performed using GenElute Mammalian Genomic DNA miniprep Kit (G1N70-1KT, Sigma, MO, USA) according to the manufacturer's guidelines and stored at −20°C until further use. For organoid and differentiated HNE samples QuickExtract DNA extraction Lucigen (ImmunoSource, QE9050, Belgium) and DNeasy Blood & Tissue Kit (Qiagen, 69506, Germany) were respectively used.

For Sanger sequencing, 400–600 base pairs around the mutation were amplified using Taq DNA polymerase (EP0404, Thermo Fisher Scientific, MA, USA) PCR with specific primers (Table S4) and purified using GenElute PCR Clean-up kit (NA1020-1KT, Sigma, MO, USA). Sanger sequencing was performed by LGC Genomics (Germany). For calculating editing efficiency, unprocessed.abi sequencing chromatograms were analyzed using EditR software[19] for graphical representation, polished reads (provided by LGC) were used unless specified otherwise.

RNA extraction and quantitative PCR

RNA was extracted from cell or organoid pellets using Aurum total RNA kit (7326820, Bio-Rad, CA, USA) and 1 μg of RNA was converted to cDNA using High Capacity cDNA Reverse Transcription kit (4368813, Thermo Fisher Scientific, MA, USA) following manufacturer's guidelines. For quantitative PCR qPCR), a LightCycler 480 SYBR Green I Master mix (4707516001, Roche Diagnostics, Belgium) containing 0.333 μM of each primer. γ-actin was used as internal control and housekeeping gene. Primer sequences are listed in Table S3. All samples were measured in triplicate of at least three biological repeats. Following PCR program was used: 95°C (10 min) – 50x [95°C (10 s) – 55°C (30 s)]. For data analysis iQ5 Optical System Software (Bio-Rad, Belgium) was used.

Immunocytochemistry

PM staining was performed as described previously.[20] For flow cytometry, cells were harvested 72 h post transfection, centrifuged at 300xg for 5 min, washed with 200 μL stain buffer (PBS - 5% FBS), centrifuged again and incubated with HA11 antibody (1:1000, #901515, Biolegend, San Diego, CA, USA) on ice for 40 min. Afterward cells were spun down, washed with 200 μL stain buffer and fixed with 100 μL ICC Fixation buffer (#00-8222-49, eBioscience, Waltham, MA, USA) for 20 min on ice. Next, 100 μL stain buffer was added, cells were spun down and washed again with 200 μL stain buffer. 50 μL secondary antibody (goat anti-mouse Alexa 488, 1:500, #A-28175, Thermo Fisher, MA, USA) was added and incubated for 30 min at room temperature. Cells were spun down, washed with 200 μL stain buffer and resuspended in 100 μL PBS for flow cytometry analysis on Guava easyCyte HT (Merck Milipore, New Jersey, USA). Percentages of PM-CFTR corrected cells were determined based on gates on the HEK293T-NT population. Since HEK293T-N1303K cells display a residual PM expression, restoration to a strong PM expression phenotype was analyzed using a "high-positive" gate, which was based on non-transfected HEK293T-N1303K cells. For both mutations, percentage of positive cells were compared with the percentage of positive cells in the respective gates of HEK293T-WT conditions (Figure S2H).

For confocal microscopy, cells were collected 24 h post transfection and seeded in 1 cm^2, poly-D-lysine (#P6407, Merck, New Jersey, USA) coated, glass-bottomed chambers (80826, Ibidi, Germany), grown for 48 h and subsequently stained for 3HA-CFTR using mouse HA11 and rabbit anti-calnexin (1:1000, #PA5-34754, Thermo Fisher Scientific, MA, USA) primary antibodies. For detection, goat-*anti*-mouse Alexa 488 (1:500, #A-28175, Thermo Fisher Scientific, MA, USA) and goat anti-rabbit Alexa 633 (1:500, #A-21070, Thermo Fischer Scientific, MA, USA) were respectively used as secondary antibodies. Nuclei were stained with DAPI (4′,6-diamidino-2-fenylindole, 1:2000, #D136, Thermo Fischer Scientific, MA, USA). Imaging was performed using Zeiss LSM 880 Airyscan confocal microscope and Zen 3.1 software.

Halide sensitive (HS) YFP quenching assay

The HS-YFP quenching assay was performed using a previously published HS-YFP construct[78] and protocol[20] with minor adaptations. Briefly, HEK293T cells were harvested 24 h post transfection and seeded in clear-bottomed 96-well plates coated with Poly-D-Lysine (P6407, Sigma, MO, USA) with a cell density of 140.000 cells per well. Transduced 16HBE cells were seeded at 30.000 cells per well in MEM +10%FBS and grown for 48 h. Cells were washed twice with DPBS supplemented with Ca^{2+} and Mg^{2+} (14040091, Thermo Fischer Scientific, MA, USA) and exposed to 10 μM forskolin (#F3917, Sigma, MO, USA) in 40 μL DMEM +2% FBS for 20 min. Fluorescence was measured using an Envision multimode plate reader (2105-0010, PerkinElmer, Zaventem, Belgium) for 5 s before and 7 s (HEK293T) or 30 s (16HBE) after I^- buffer (137 mM NaI, 2.7 mM KI, 1.7 mM KH_2PO_4, 10.1 mM Na_2HPO_4, 5 mM D-glucose, Sigma, MO, USA) was injected. CFTR function relative to WT and measured by HS-YFP quenching was determined as $1\text{-}F/F_0$.

Western blot

HEK293T protein samples for western Blot analysis were collected 72 h post transfection. Culture medium was aspirated, cells were washed with 1 mL PBS and lysed with 1% sodium dodecyl sulfate (SDS, 05030-2.5L-F, Merck Life Sciences, Germany) in PBS containing complete protease inhibitor (cat# 11873580001, Roche, Switzerland). Cell lysates were mechanically homogenized using 1mL needles (LBTV1E, Merck Life Sciences, Germany). To assure equal loading, protein concentrations were measured using the bicinchoninic acid assay (BCA protein assay kit, 23225, Thermo Fisher Scientific, MA, USA) and spectral readout at 540 nm via Anthos 2010 Microplate reader. Loading dye, consisting of 200 mM Tris-HCl (RES3098T-B103X, Sigma, MO, USA), 400 mM dithiothreitol (GE17-1318-02, Sigma, MO, USA), 8% SDS, 40% glycerol and 0.5% bromophenol blue (B7021, Sigma, MO, USA) was added to 15 μg of protein. The samples were incubated at 37°C for 15 min. Polyacrylamide gel electrophoresis (PAGE) was run on a 3–8% Tris-Acetate polyacrylamide gel (NuPage, WG1602A, Thermo Fisher, MA, USA) for 50 min at 150V with Tris-Acetate SDS 1x running buffer (215682500, Thermo Fisher Scientific, MA, USA). PageRuler protein ladder (26616, Thermo Fisher Scientific, MA, USA) was included to estimate protein sizes. After PAGE, the gel was blotted on a methanol activated (20846.361, VWR, PA, USA) polyvinylidene difluoride membrane (PVDF, Trans-Blot, Turbo RTA Midi PVDF Transfer Kit, 1704273, Bio-Rad, CA, USA) using Trans-Blot Turbo Transfer System (1704150, BioRad, CA, USA) for 15 min at 2.5 A. The membrane was blocked using 5% milk powder in 0.1% Triton/PBS for 30 min and followed by overnight incubation with primary antibodies against the hemagglutinin tag (HA11, 1:1000), against CFTR (1:1000, CFF Ab mix 570 + 596+660) and against α-tubulin (1/2000, Sigma, MO, USA). Next, the PVDF membranes were washed three times with 0.1% Triton/PBS for 10 min before incubation with secondary goat-*anti*-mouse horseradish peroxidase conjugated antibodies (1:10.000, P044701-2, Agilent, CA, USA) for 1h at room temperature. After washing three times, the blot was imaged using Clarity Western ECL substrate (#1705061, Bio-Rad, CA, USA) and Amersham ImageQuant 800 Fluor (GE Healthcare, IL, USA). Raw,

unprocessed blots are shown in Figure S10. The relative amount of band C on western blots was quantified using ImageQuant TL software (GE Healthcare, IL, USA) and expressed as the intensity of band C/(band B + band C).

Rectal organoid transduction and forskolin induced swelling (FIS) assay

Human rectal organoids were generated from rectal biopsies of PwCF as previously described[80] and biobanked following successful culture. Informed consent was obtained prior to biopsy collection, in accordance with the ethical committee of UZ Leuven (S56329, S67338). Specifically, biobanked samples from PwCF homozygous or heterozygous for L227R (L227R/L227R, L227R/F508del) or N1303K (N1303K/N1303K, N1303K/F508del, N1303K/3121-1A>G) were used for this study.

For transduction, organoids were trypsinized to single cell using Trypsin 0.25% EDT for 10 min at 37°C. 15.000 cells were resuspended with 25 μL lentiviral vector mix and incubated for 10 min at room temperature, as described previously.[33] Next, the cell-vector suspension was embedded in 25 μL ice-thawed Matrigel (356231, Corning, New York, USA) which was used to plate 5 μL droplets in 96 well plates in octuplicate for each condition.[80] Matrigel domes were allowed to polymerize for 10 min at 37°C and subsequently submerged in human medium supplemented with Rock inhibitor (Y-27632, #S0149, Selleckchem, TX, USA) for the first three days to allow outgrowth from single stem cells. Organoids were allowed to grow for fourteen days. For FIS, medium was changed every 2–3 days. Organoid medium was replaced by medium containing 5 μM Forskolin 14 days after transduction. Organoid swelling was immediately monitored by live, label-free imaging (LSM800, Zeiss, Germany) at 37°C and 5% CO_2 as described previously.[13] Images were taken every 10 min over the course of 2 h.

Machine learning algorithms for automated FIS analysis

DETE*C*TOR (Detection of Targeted Editing of *CFTR* in Organoids) consists of machine-learning (ML) models trained to perform two tasks: 1) identify the total number of organoids in a given plane and 2) analyze their swelling properties between two images taken during a time course experiment. For the first model, an algorithm previously used for dense people crowd counting tasks was adopted (Bayesian Crowd Counting).[83–85] LabelMe software[86] was used to annotate 18.499 organoids (116 8-bit brightfield images). The images presented with different organoid genotypes, sizes, amount of overlap, focus and swelling. A VGG19 model[87] learned the organoid phenotypes' prior information using the Gaussian kernel with density map and Bayesian loss function to estimate the background likelihood.[88] The algorithm estimates the position of each organoid condition independently so that the total number of organoids is calculated accurately, overcoming the interference of overlapping.

For the second task, to detect the swelling of the identified organoids, the YOLOv7 algorithm[89] was used. To extract the dynamic behaviors, single time frame sequences were preprocessed (with shadow removal and filtering) and subjected to frame differencing (Figure S5A). Based on organoid swelling movies, 4.093 organoids were labeled on 113 frame differencing images. These were subsequently used to train a YOLOv7-E6E model.[89] Taking expert-labelled images as ground truth, we evaluated the first task with Mean Absolute Error (MAE) and Mean Squared Error (MSE); and the second task with Average Precision at the intersection over union threshold 0.5 (AP_{50}). To test the time performance, we locally deployed the whole program with two trained ML models. We processed the analysis of a 96 well plate experiment with images taken every 10 min for 2 h (=1152 brightfield images 512 x 512 pixels). On a workstation (Intel Core 13900K CPU, single Nvidia RTX 3090 GPU) the complete analysis took 39s. Code, trained models and guidelines to run DETE*C*TOR have been deposited to Dataverse (https://doi.org/10.7910/DVN/OZZRPG) and Github (https://github.com/RL-arch/detector).

Primary nasal epithelial cell culture

Human nasal epithelium (HNE) cells from pwCF harboring L227R or N1303K alleles (L227R/L227R and N1303K/R1162X, $n = 1$ each) were collected and biobanked as previously described.[55] Written informed consent was obtained from each adult PwCF or parent for those aged 12 to 18 years (AFSSAPS (ANSM) B1005423–40, n° Eudract 2010-A00392-37; CPP IDF2: 2010-05-03-3). HNE cells were thawed and cultured using collagen IV coated flasks (C7521, Merck, New Jersey, USA) and commercial expansion medium (Pneumacult-Ex Plus, #05040, StemCell Technologies, Canada). At passage 3, 100.000 cells were transduced in suspension for 10 min at room temperature with 50 μL LV vector mixes containing equal titers of LV-PE2 + LV-epegRNA + LV-ngRNA (PE3) or LV-PE2 + LV-epegRNA + LV-ngRNA + MLH1dn (PE5). Immediately after transduction, cells were seeded on collagen IV coated 0.4 μm pore transwells (Corning 6.5 mm polyester, #3470, Fisher Scientific, MA, USA) and expansion medium was added to both compartments. Cells were cultured in submerged mode for 2–4 days at 37°C and 5% CO_2. When complete confluency was reached, HNEs were put on air-liquid interface (ALI) by removing the apical medium and switching to differentiation medium (Pneumacult, 05001, StemCell Technologies, Canada) for the basolateral compartment. After three weeks, HNE monolayers achieved full differentiation as evidenced by mucus secretion and mucociliary beating.

Ussing chamber measurements

For short-circuit current (I_{sc}), transwells containing differentiated HNE monolayers were inserted into an Ussing device (EVC4000 Precision V/I Clamp, World Precision instruments; Labchart v8.1 software, ADInstruments) with chloride gradient between both chambers. Ussing measurement was performed as previously described[55] with identical buffer compositions. All compounds were acquired from Merck (Fallavier, France) and dissolved in DMSO before frozen storage. After stabilisation of baseline I_{sc}, 100 μM amiloride was added to inhibit apical sodium absorption by epithelial Na^+ channel (ENaC). CFTR activation was apically and

basolaterally stimulated using cAMP-agonists forskolin (10 μM) and 3-isobutyl-1-methylxanthine (IBMX, 100 μM). Upon stable baseline, 10 μM Inh172 a specific CFTR-inhibitor was added to the apical side to investigate CFTR-specific currents. Lastly, 100 μM ATP was applied to induce purinergic calcium-dependent chloride secretion as indication for epithelial integrity and viability.

Histological staining

The HNE monolayers were fixed with 4% paraformaldehyde (1.04003.1000, Sigma Aldrich, MI, USA) and embedded in paraffin. 5μm sections were cut and mounted on Superfrost Plus slides (J1800AMNZ, Thermo Fisher Scientific, MA, USA) and stained with either hematoxylin and eosin (Abcam ab245880) or Periodic Acid-Schiff stain (395B, Sigma Aldrich, MI, USA) according to manufacturer's protocol. After staining, the slides were covered with DPX (06522, Sigma Aldrich, MI, USA) and a glass coverslip (630–2603, VRW, PA, USA). Brightfield images ware taken using the Leica DM6B (DFC7000T) microscope.

Immunofluorescence staining

After deparaffinization with xylene (534056, Merck Life Science, New Jersey, USA) and 100% ethanol (VWR 85823360), antigen retrieval was performed by cooking the 5μm paraffin sections for 20 min in HIER buffer (AB208572, Abcam). First, the slides were subjected to peroxidase quenching by incubation in 0.3% H_2O_2 (CL00.2306.1000, Chem-Lab) in PBS for 15 min at RT, then blocked for 1h in 10% Goat serum (S26, Merck Life Science) in PBS. Afterward, the slides were incubated overnight at 4°C with primary antibodies (diluted in blocking solution) targeting the different epithelial cell-markers: mouse anti-beta-tubulin (T7941; 1/4000 diluted, Sigma Aldrich, MI, USA), Mouse –anti-MUC5AC (ab3649; 1/1600 diluted, Abcam) and Mouse –anti-Cytokeratin 5 (NCL-L-CK5; 1/500 diluted, Leica Biosystems). Sections were incubated for 1h at RT with Goat-*anti*-Mouse HRP secondary antibody (P0447; 1/200 diluted, Agilent) followed by incubation for 10 min at RT with fluorescent CF 647 dye (96022, Biotium, CA, USA) diluted 1/200 in 100 mM borate buffer (Fisher Scientific J63742.AK) + 0.003% H_2O_2. Finally, the sections were stained with 1μg/μL DAPI solution (D1306, Life Technologies) diluted 1/4000 in PBS. Conventional immunofluorescent staining was used to visualise uteroglobin: after antigen retrieval, the slides were incubated overnight at 4°C with rat-*anti*-uteroglobin (MAB4218; 15μg/ml diluted in blocking buffer, R&D Systems) followed by incubation with Goat-anti rat Alexa 555 secondary antibody for 1h at RT (A21434; 1/1000 diluted in blocking buffer, Invitrogen). Finally, the sections were stained with 1μg/μL DAPI solution diluted 1/4000 in PBS and mounted with mowiol and a glass coverslip. Fluorescent images were taken using the Leica DM6B (DFC7000T) microscope.

In silico prediction of potential off-targets

For in silico identification of off-target (OT) sites, CRISPOR[40] was used. CRISPOR is an online available tool (http://crispor.tefor.net) that leverages the Doench and Moreno-Mateos models that were trained on large experimental datasets to estimate sites with increased propensity for SpCas9 OT activity.[41] Spacer sequences of optimized pegRNAs and ngRNAs with their respective full PAMs were give as input, *Sp*Cas9 was selected as nuclease and "Homo Sapiens – UCSC Dec. 2013 (GRCh38/hg38) + SNPs: dbSNP148, Kaviar" was used as reference genome. Identified sites with sequence similarity were downloaded and ranked based on Cutting Frequency Determination score.[41]

Experimental identification of potential off-targets via GUIDE-Seq

Genome-wide, Unbiased Identification of DSBs Enabled by Sequencing (GUIDE-Seq) was performed as previously described.[33] In short, HEK293 cells were transfected with 500 ng of *Sp*Cas9 plasmid (pX-Cas9[90]), 250 ng of L227R-CFT/N1303K-CFTR pegRNA/ngRNA plasmid, 10 pmol of double-stranded oligodeoxynucleotides (dsODNs) and 50 ng pEGFP-IRES-puro plasmid using Lipofectamine 3000 (L3000008, Thermo Fisher Scientific, MA, USA). 24h after transfection, cells were split and selected with puromycin. Genomic DNA was extracted (DNeasy Blood and Tissue kit, #69506, Qiagen, Hilden, Germany) and sheard to average length of 500 bp using sonication (Focused-ultrasonicator, Covaris, MA, USA). End-repair and sequencing adaptor ligation were performed using NEBNext Ultra End Repair/dA Tailing Module (E7546S, New England Biolabs, MA, USA) and NEBNextUltra Ligation module (E7595S, New England Biolabs, MA, USA) respectively following the procedures reported by Nobles et al.[91] Amplification was performed as described by Tsai et al.[42] and libraries were quantified using Qubit dsDNA High Sensitivity Assay kit (Q33233, Thermo Fisher Scientific, MA, USA). Next-generation sequencing was performed on an Illumina MiSeq sequencing device using Illumina Reagent kit V2-150PE.

Raw sequencing data were processed and analyzed using the GUIDE-Seq (v1.0.2) command line utilities.[42] In short, files were demultiplexed and umi (unique molecular identifier) tagged. PCR duplicates were identified and consolidated, reads were aligned to GrCh38 using BWA-MEM. When dsODNs integrations were identified, the genomic region was retained as off-target cleavage site if at least 13 base pairs matched with the spacer of the pegRNA or ngRNA and if absent in the background control. Raw sequencing reads have been submitted to NCBI-SRA.

Targeted deep sequencing

For evaluation of potential OT activity, genomic DNA was extracted from HEK293T cells three days post transfection with PE plasmids or from patient-derived organoids fourteen days post transduction. For these samples GenElute Mammalian Genomic DNA miniprep Kit (G1N70-1KT, Sigma, MO, USA) and Lucigen Quickextract (QE09050, Immunosource, Schilde, Belgium) kits were used respectively.

Loci identified as potential off-targets either via *in silico* prediction or via experimental identification by GUIDE-Seq were PCR-amplified using iProof High-Fidelity polymerase (#172–5302, Bio-Rad, CA, USA) and adaptor-containing primers (Table S3). PCR amplicons were purified using Ampure XP beads (A63881, Analis, Belgium) and 1.2 sample-beads ratio. Qubit (High Sensitivity kit, 10616763, Fisher Scientific) was used to measure DNA concentration. Indexing PCR was performed with Phusion High Fidelity PCR master Mix with HF buffer (M0531S, Bioké), followed by Ampure bead purification. Fragment Analyzer (NGS Fragment High Sensitivity Analysis Kit 1–6000 bp, DNF-474-500, Agilent) was used before and after indexing PCR to confirm fragment length. Amplicon molarities were determined via qPCR (Kapa SYBR FAST Universal qPCR kit + Primer premix + Illumina DNA standards, 7960140001/CM7079, Roche, Basel, Switzerland) and sequenced using NovaSeq 6000 S4 Reagent Kit v1.5 (300 cycles; 20028312, Illumina, SA, USA).

Samples were sequenced on a NovaSeq 6000 (Illumina, CA, USA), 150 cycles (150 bp paired-end). Raw sequencing data were analyzed using command-line utilities of CRISPResso2 (v2.2.7)[79] in batch mode (CRISPRessoBatch) with following settings: –plot_window_size 1 –amas 50 –default_min_aln_score 50 -s 10 -q 10 –exclude_bp_from_left 5 –exclude_bp_from_right 5. A number of sites picked up by GUIDE-seq corresponded to (semi)repetitive regions in the genome that led to convoluted amplicons. Amplicons mapping to the originally identified genomic coordinates were separated using the CRISPRessoPooled pipeline preceding submission to CRISPRessoBatch. The full batch files for analysis at expected DSB and PE sites can be found in Tables S5 and S6. Raw sequencing reads have been submitted to NCBI-SRA.

QUANTIFICATION AND STATISTICAL ANALYSIS

Statistical analyses were performed using GraphPad (Prism9). Parametrical, unpaired/unpaired Student's t test (with/without Welch's correction), Mann-Whitney U t-test or one-way ANOVA with Sidak's correction for multiple comparison and Tukey's multiple comparison test were used to analyze differences between experimental conditions. Two-sided tests were used unless otherwise specified. Pearson or Spearman correlation were used to investigate the relation between genomic and protein/function level readouts. Results are shown as mean ± standard deviation. p-values were denoted as follows: * ($p < 0.05$), ** ($p < 0.01$), *** ($p < 0.001$), or **** ($p < 0.0001$). Test specifications are mentioned in figure legends. Datapoints on graphs depict biological repeats.